
ELECTROMAGNETIC DIAGNOSTICS OF ATMOSPHERIC PLASMAS

**Frank T. Djuth
John H. Elder**

**Geospace Research, Inc.
550 N. Continental Boulevard, Suite 110
El Segundo, CA 90245**

March 2000

**Final Report
September 1994 – July 1999**

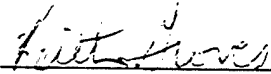
Approved for Public Release; Distribution Unlimited



**AIR FORCE RESEARCH LABORATORY
Space Vehicles Directorate
29 Randolph Rd
AIR FORCE MATERIEL COMMAND
Hanscom AFB, MA 01731-3010**

20020827 014

This technical report has been reviewed and is approved for publication



Keith Groves
Contract Manager



John Hecksher, Lead, Ionospheric
Hazards Specification & Forecast Team

Qualified requestors may obtain additional copies from the Defense Technical Information Center (DTIC). Other requests shall be referred to AFRL/VS BXI

If your address has changed, if you wish to be removed from the mailing list, or if the address is no longer employed by your organization, please notify AFRL/VSOSTI, 29 Randolph Road, Hanscom AFB, MA 01731-3010. This will assist us in maintaining a current mailing list.

Do not return copies of this report unless contractual obligations or notices on a specific document require that it be returned. Destroy by any means that will prevent disclosure of contents or reconstruction of this document.

REPORT DOCUMENTATION PAGEForm Approved
OMB No. 0704-0188

Public reporting burden for this collection of information is estimated to average 1 hour per response, including the time for reviewing instructions, searching existing data sources, gathering and maintaining the data needed, and completing and reviewing the collection of information. Send comments regarding this burden estimate or any other aspect of this collection of information, including suggestions for reducing this burden, to Washington Headquarters Services, Directorate for Information Operations and Reports, 1215 Jefferson Davis Highway, Suite 1204, Arlington, VA 22202-4302, and to the Office of Management and Budget, Paperwork Reduction Project (0704-0188), Washington, DC 20503.

1. AGENCY USE ONLY (Leave blank)		2. REPORT DATE 02 March 2000	3. REPORT TYPE AND DATES COVERED Final Report, 22 Sep 1994 through 31 July 1999	
4. TITLE AND SUBTITLE Electromagnetic Diagnostics of Atmospheric Plasmas			5. FUNDING NUMBERS PE 62601F PR ARPA TA GH WW AA Contract F19628-94-C-0101	
6. AUTHOR(S) Frank T. Djuth and John H. Elder				
7. PERFORMING ORGANIZATION NAME(S) AND ADDRESS(ES) Geospace Research, Inc. 550 N. Continental Boulevard, Suite 110 El Segundo, CA 90245			8. PERFORMING ORGANIZATION REPORT NUMBER GRI-BA-00-7250	
9. SPONSORING / MONITORING AGENCY NAME(S) AND ADDRESS(ES) Air Force Research Laboratory 29 Randolph Road Hanscom AFB, MA 01731-3010 Contract Manager: Keith M. Groves/GPIA			10. SPONSORING / MONITORING AGENCY REPORT NUMBER AFRL-VS-TR-2000-1522	
11. SUPPLEMENTARY NOTES				
12a. DISTRIBUTION / AVAILABILITY STATEMENT Approved for public release; distribution unlimited			12b. DISTRIBUTION CODE	
13. ABSTRACT (Maximum 200 words) This research program addresses fundamental issues related to the interaction of a high-power, high-frequency (3 - 10 MHz) radio wave with the ionosphere. Data acquired at the High-Power Auroral Stimulation (HIPAS) Observatory in Fairbanks, Alaska was used to study the formation of artificial periodic inhomogeneities (API) in the lower and upper atmosphere. Quite remarkably, the API echoes are observed as low as the polar stratopause near 45 km altitude. The meteor-like nature of the echoes open new vistas for atmospheric research in the middle atmosphere. A second investigation focused on the physics of missile plumes in the lower atmosphere. This can be viewed as a lower atmosphere modification experiment in which missile fuel generates a highly collisional plasma. Plumes from Aries rockets launched from NASA Wallops Island Flight Facility, Virginia were simultaneously monitored with radars operating at 139 MHz, 50 MHz, 430 MHz, and 2840 MHz. Absolute plume cross section and spectral signature were the measured quantities of primary interest. Additional research entailed studies of the equatorial ionosphere, investigations of upper atmosphere lightning flashes, and an examination of ion and Langmuir oscillations excited by the high-frequency, ionospheric modification facility at Tromsø, Norway.				
14. SUBJECT TERMS Ionospheric modification, High-power radio waves, Missile plumes, Equatorial ionosphere, Sprites and blue jets, Radar processor			15. NUMBER OF PAGES 43	
			16. PRICE CODE	
17. SECURITY CLASSIFICATION OF REPORT Unclassified	18. SECURITY CLASSIFICATION OF THIS PAGE Unclassified	19. SECURITY CLASSIFICATION OF ABSTRACT Unclassified	20. LIMITATION OF ABSTRACT SAR	

TABLE OF CONTENTS

1.	Objectives and Goals of the Research Program.....	1
2.	HF Ionospheric Modification Research at HIPAS Observatory.....	1
2.1	Introduction.....	2
2.2	Experiment Description.....	5
2.3	HIPAS Observations.....	6
2.4	Discussion.....	19
2.5	Conclusions.....	22
2.6	Future Experiments.....	23
3.	Rocket Plume Studies from Wallops Island Flight Facility, Virginia.....	24
3.1	Background.....	25
3.2	Radar Software and Hardware.....	26
3.3	Radar Parameters.....	27
3.4	Rocket Plume Observations.....	28
4.	Equatorial Experiments from Chile.....	31
5.	Sprite/Blue Jet Campaign from Colorado.....	31
6.	HF Modification Experiment at Tromsø, Norway.....	32
6.1	Background.....	33
6.2	Initial Results.....	35
7.	Radar Processor Upgrade.....	38
7.1	File Structure.....	39
7.2	Input Voltage Range.....	39
	References.....	40

1. Objectives and Goals of the Research Program

Several tasks were performed under contract F19628-94-C-0101. The first entailed studies of the interaction of a powerful, high-frequency (HF) radio wave transmitted from the ground into the ionosphere. The overall goal was to achieve a more complete understanding of artificial periodic inhomogeneities generated in the middle and upper atmosphere. An additional investigation focused on the physics of missile plumes in the lower atmosphere is also discussed in this report. This can be viewed as a lower atmosphere modification experiment in which missile fuel generates a highly collisional plasma. Plumes from Sergeant and Aries rockets launched from NASA Wallops Island Flight Facility, Virginia were simultaneously monitored with radars operating at 139 MHz, 50 MHz, 430 MHz, and 2840 MHz. Absolute plume cross section and spectral signature were the quantities of primary interest.

Other research topics addressed as part this program include the formation of ionospheric irregularities near the geomagnetic equator, the physics of upper atmospheric lightning flashes known as sprites and blue jets, and the temporal development of Langmuir and ion oscillations produced by the high-power HF facility at Tromsø, Norway. Additional efforts were made to update the radar processors originally built for the HF Active Auroral Research Program (HAARP).

2. HF Ionospheric Modification Research at HIPAS Observatory

In this section, results are presented from experiments that employ high-power, high-frequency (HF) radio waves to probe the mesosphere and lower thermosphere. The measurements were made at the High-Power Auroral Stimulation (HIPAS) Observatory located near Fairbanks, Alaska. One objective of the study was to determine the feasibility of using artificial electron density perturbations created in the auroral environment to measure the properties of the background neutral gas from ~50 km to ~120 km altitude. The observing technique relies on the production of so-called "artificial periodic inhomogeneities" (API) in the altitude region(s) of interest. These induced irregularities are believed to be horizontally stratified and conform to the standing wave pattern produced by the reflection of the powerful HF wave in the ionosphere. In the *D* region above HIPAS, API decay curves are strictly exponential and the phase histories are strictly linear. On occasion, echoes are detected at very low altitudes (~45 km) in the vicinity of the polar stratopause. The API backscatter at HIPAS is often superimposed on regions of partial reflection, auroral *E*, and sporadic *E*. Information about ambipolar diffusion rates and electron attachment to O₂ is obtained by measuring the relaxation time of the induced irregularities. In general, API phase velocities below ~95 km altitude appear to be related to vertical neutral motions. However, detailed validation studies throughout the mesosphere have not yet been performed at HIPAS or any other API facility. At altitudes between ~45 and ~80

km, high-resolution observations at HIPAS reveal the presence of sharply defined bands of API scatter 15-20 km in altitude extent. The existence of such bands and their fluctuation in altitude cannot be explained within the context of existing theory. Large variations in API backscatter power (10-20 dB) are typically observed in the *D* region over time scales of 30 s or less. Most likely this is caused by fading in the ionospherically-reflected component of the standing wave pattern. Finally, power stepping studies reveal a roughly linear relationship between *D* region backscatter power and HF power. Fundamental questions related to the horizontal dimension of the API patch and its spatial structure remain to be addressed in future experiments.

2.1 Introduction

Artificial Periodic Inhomogeneities (API) refer to a type of plasma irregularity produced by large ground-based, high-frequency (HF) modification facilities. API are believed to conform to the standing wave pattern of the modifying HF beam and are generally assumed to be horizontally stratified. Both the modification transmissions and the diagnostic transmissions are usually made in the vertical direction from co-located or closely spaced facilities. API irregularities have been detected at altitudes ranging from ~50 km to the point of reflection of the modifying HF wave. High-power waves having either X-mode or O-mode polarization can be used to generate the horizontally-stratified irregularities. However, the effectiveness of excitation at various altitudes is dependent on wave polarization. Because API can be excited over a wide range of background plasma parameters, different types of plasma forcing processes are invoked to explain API production in various regions of the ionosphere/atmosphere.

The first observations of API in the ionospheric *F* region are described and interpreted by *Belikovich et al.* [1975]. These measurements were made with the Zimenki HF facility located near Nizhny Novgorad (formerly Gor'kii), Russia. In this case, a 4.6-MHz, O-mode modification wave was continuously transmitted, and pulsed diagnostic transmissions were made with a separate HF system operating at 5.6 MHz with X-mode polarization. Backscatter occurs if the wavelength of the API is equal to half the wavelength of the diagnostic pulsed transmission. At *F*-region heights, API are believed to be driven by ponderomotive forces produced either by the standing wave pattern of the modifying HF wave alone or, in the case of O-mode transmissions, by the combined ponderomotive forces of the electromagnetic wave and excited Langmuir oscillations. Because the dependence of refractive index on electron plasma frequency is different for O- and X-mode waves, wavelength matching conditions are satisfied at dissimilar frequencies when O-mode waves are used for modification and X-mode transmissions are employed for diagnostic purposes. For typical *F* region parameters, the difference between the O-mode and X-mode frequencies range from ~0.5 to 1.0 MHz near the reflection height of the modifying HF wave. Thus, it is possible to continuously diagnose API in one, or at most two, altitude regions [e.g., *Belikovich et al.*, 1977] using a diagnostic frequency that is substantially different from the

modification frequency. At altitudes far below the HF reflection height, the frequency difference becomes much smaller.

The early Russian *F*-region results were reproduced at Arecibo Observatory, Puerto Rico nearly a decade later by *Fejer et al.* [1984]. The technique of setting the probe signal to X-mode polarization and using O-mode polarization for the modifying wave was also adopted at Arecibo. These observations verified that wavelength matching conditions are necessary for API detection. The synchronism required between the O-mode/X-mode modification and diagnostic waves provides strong evidence that the HF standing wave pattern plays a prominent role in API excitation at *F* region heights. However, API must coexist with other HF-induced irregularities, which can degrade the standing wave pattern. Ionospheric inhomogeneities distort the phase front of the modifying HF wave and in so doing deform the API lattice. Moreover, instability processes can extract energy from the HF pump wave near reflection leading to a much weaker downcoming wave. This reduces the envelope of the HF standing wave, which serves as a forcing agent for API. The impact of HF-induced irregularities on API has been examined theoretically by *Borisov and Varshavskiy* [1982]. They conclude that API amplitudes can be considerably weakened by HF-induced perturbations having transverse scale sizes comparable to the modification wavelength.

In the *F* region experiments of *Belikovich et al.* [1975] and *Belikovich et al.* [1977], the growth and decay time constants of backscatter amplitudes from API were reported to be of the order of 20-30 ms. Both time constants are dependent in part on the vertical wavelength of the excited API. In the above case, the high-power transmissions were made at 4.6 MHz with O-mode polarization, whereas probing pulses were transmitted at 5.6 MHz with X-mode polarization. In this case, one finds that the diagnosed API wavelength is ~ 67 m. Additionally, oscillations in echo intensity with periods ranging from 50 ms to 70 ms are reported by *Belikovich et al.* [1977]. Decay constants are interpreted in terms of Landau attenuation, whereas the oscillations are attributed to Landau damped ion-acoustic waves [*Belikovich et al.* 1977]. The API electron density perturbation $\Delta N_e / N_e$ is calculated by *Belikovich et al.* [1977] to be $\sim 10^{-6}$, but this estimate is revised by *Fejer et al.* [1984] to $\sim 10^{-4}$.

The application of API to measurements of ionospheric electron density profiles is demonstrated by *Belikovich et al.* [1978a]. In comparison to ionosonde measurements, the API approach simplifies the derivation of the actual profile and supports direct measurements in the ionization trough between the *E* and *F* regions. Measurements of API in the trough region were first reported by *Belikovich et al.* [1978b]. In contrast to the *F*-region studies noted above, these experiments were performed with O-mode diagnostic transmissions and an X-mode modification wave. More recent observations of electron density profiles between ~ 95 km and 180 km altitude are presented by *Belikovich et al.* [1995].

Belikovich et al. [1978b] assess the relative importance of API excitation by electron thermal and ponderomotive (striction) forces in the *E* and *F* region ionosphere. Ponderomotive forces are dominant in the *F* region, but thermal forces become important at lower heights. The contributions of electron thermal and striction forces to the formation of API are shown to be comparable at ~110 km altitude. In addition, below ~120 km the damped oscillatory process used to describe periodic API intensity fluctuations in the upper *F* region is replaced by a transitional process, which gives rise to aperiodic fluctuations. The reported *E* region measurements were made with an X-mode modification wave at a frequency of 5.75 MHz. O-mode diagnostic pulses were transmitted at 5.65 MHz. In this case, the wavelength of the detected API is ~27 m. The amplitude decay constant measured at altitudes near 120 km (~40 ms) is attributed to ambipolar diffusion. It is suggested that other factors such as turbulent neutral motions may influence the API decay constant below 90 km altitude. Overall, the authors stress the potential use of API echoes to measure background ionospheric parameters such as electron temperature, ambipolar diffusion rate, and electron density. A detailed methodology for determining electron and ion temperatures and the ion-neutral collision frequencies at altitudes between ~160 and 210 km is offered by *Belikovich et al.* [1986].

The first experimental observations of API in the lower *D* region were made by *Belikovich et al.* [1981]. In this case, modification frequencies of 5.75 MHz and 3.0 MHz were used, both of which had X-mode polarization. A separate partial reflection facility was used for diagnostic measurements. Backscatter from API was observed when the frequency of the probing transmitter matched that of the modification wave. Characteristic decay times of the irregularities range from 0.1 - 1.0 s at altitudes between ~50 km and 70 km. The formation of API in this region of the atmosphere is attributed to changes in the negative ion (principally O_2^-) attachment/detachment chemistry brought about by electron heating. In particular, it is hypothesized that the electron-temperature dependence of the detachment process gives rise to the inhomogeneities, and the rapid decrease in electron temperature at HF turn-off leads to API decay via re-attachment. A more complete description of ionization balance in a *D*-region plasma consisting of negative and positive ions and electrons is provided by *Belikovich and Benediktov* [1986a] and *Belikovich and Razin* [1986]. *Belikovich and Benediktov* [1986a] employ API decay constant τ in the lower *D* region to determine the ratio of negative ions to electrons λ at altitudes between 55 and 78 km. Experimental measurements are combined with a simplified model to probe seasonal variations in the *D* region chemistry. Brief fluctuations in API decay constants are attributed to dynamic changes in air pressure and temperature caused by the passage and dissipation of gravity waves. Systematic changes in τ at sunrise and sunset are interpreted by *Belikovich and Benediktov* [1986b] in terms of variations in the concentrations of O and excited $[O_2^1\Delta_g]$. Additionally, changes in solar UV and visible radiation give rise to distinctive changes in

echo amplitude versus altitude. Finally, the influence of neutral temperature on τ is examined by *Belikovich and Benediktov* [1986c]. Measured fluctuations in τ are explained in terms of changes in λ brought about by neutral temperature variations. Temperature changes associated with gravity waves are used to interpret these observations and provide the basis for predicted variations in echo amplitude.

Extensive investigations of API with the HF facility at Tromsø, Norway are reported by *Rietveld et al.* [1996]. The observations represent the first measurements of API at a high-latitude station. Most of the data presented by *Rietveld et al.* focuses on API in the *D* and *E* regions of the ionosphere. Echoes at altitudes as low as 52 km are shown. The vertical phase velocities deduced for the phase histories of API echoes are compared with incoherent scatter measurements made with the VHF radar. It is concluded that some of the API-derived velocities in the 75-115 km height range appear consistent with vertical neutral winds as indicated by their magnitudes and also that there may be evidence of gravity waves. Other data in the 50-70 km range show an unrealistically large bias. It proved difficult to obtain both API and incoherent scatter radar (ISR) velocities with overlapping altitudes. Some uncertainty is expressed by the authors as to whether the ISR and API were measuring the same quantities.

Rietveld et al. also compared API decay time-constants and amplitudes between 53 and 70 km with the results of an ion-chemistry model. The calculated amplitudes show good agreement with the data in that the maximum occurs at about the same height as that measured. The calculated time-constant agrees very well with the data below 60 km but is larger above 60 km by a factor of up to 2 at 64 km.

API results from HIPAS Observatory are presented below.

2.2 Experiment Description

A limited API campaign was performed at HIPAS Observatory during the period September 18, 1995 through September 28, 1995. A detailed description of the HF modification facility is provided by *Wong et al.* [1990] and *Wong and Brandt* [1990]. Observations were made near sunset between 16:00 - 22:00 LT (01:00 - 07:00 UT) on all days within the campaign period. HIPAS is located north of Fairbanks, Alaska (64.9° N, 146.8° W); its geomagnetic latitude (64.8° N) is slightly less than Tromsø, Norway (66.9° N), but the geomagnetic dip angles of HIPAS and Tromsø, Norway are approximately the same (~77-78°). The dip angle plays an essential role in HF-driven instabilities responsible for the formation of short-scale, geomagnetic, field-aligned irregularities [e.g., *Djuth et al.* 1985]. In this important respect, the two locations are equivalent. The observations reported below were made under quiet geomagnetic conditions ($K_p \leq 2$). Indeed all campaign observations were made under quiet conditions with the exception of a three-hour data segment on September 26, 1995 when K_p was 3-. In general, the data presented here are representative of other observations made during the campaign period.

Our focus on *D*-region API scatter required that the frequency of probe transmissions match that of the modification wave so that wavenumber matching conditions could be satisfied. The observing strategy involved the use of a long modification pulse to excite the API. This was followed by a series of diagnostic pulses, which were used to simultaneously monitor the decay of API echoes at all altitudes. A modification wave having O-mode polarization was selected to optimize the HF standing wave pattern. It was assumed that reductions in *D* region absorption (compared to those anticipated for X-mode polarization) would greatly outweigh losses from anomalous absorption near the reflection point.

All HF transmissions were made at 2.85 MHz with O-mode polarization. Diagnostic pulses $\sim 10\ \mu\text{s}$ in length were transmitted from the HIPAS facility yielding an altitude resolution of 1.5 km. The receiver station was located approximately 1 km away from the HIPAS HF array. A half-wave dipole was used as a receiving antenna. As a result, half of the ionospherically reflected/scattered HF power was automatically discarded on reception. Ionospheric signals were routed to an analog HF receiver having complex voltage channels at baseband. The receiver outputs were digitally sampled and related "housekeeping" data were recorded with a high-speed radar processor. Although raw voltage data were used for detailed analyses, limited amounts of the incoming data were processed and displayed in real time to help guide the experiment.

Figure 1 illustrates the sequence of HF transmissions used for the observations. Each 30-s frame begins with a 10-s transmission used for modification. This is followed by a series of 10- μs diagnostic pulses transmitted within a 5 ms interpulse period. The pulsing continues for 17 s, after which there is a 3-s HF-off period. This 30-s cycle was continuously repeated during an observation period. For all observations (except those involving HF power stepping), it is estimated that ~ 40 MW effective radiated power (ERP) was transmitted during the 10-s modification pulse, and that the ERP of the diagnostic pulses was ~ 20 MW.

2.3 HIPAS Observations

During the HIPAS experiments, the ionospheric return signals were sampled at $4\ \mu\text{s}$ intervals (600-m increments) across the altitude interval 34.8 km - 341.4 km. A typical example of a range-time-intensity display obtained after HF turn-off is shown in Figure 2. Although the ordinate of Figure 2 labeled "altitude" is appropriate for *D* region API, a more suitable term for *F* region phenomena is "virtual height," because of the large group delays that develop near the point of radio wave reflection. The strong return between 206 km and ~ 250 km virtual height arises from the specular reflection of the diagnostic pulses in the *F* region. The gain of the HF receiver was set for maximum sensitivity to aid in the detection of weaker signals in the *D* region. Consequently, the strong specular return from the *F* region saturates the receiver. After about $350\ \mu\text{s}$ (~ 50 km range), the receiver begins to recover. During the recovery phase the receiver rings, giving rise to layer-like artifacts at altitudes between ~ 250 km and 300 km. This structure changes

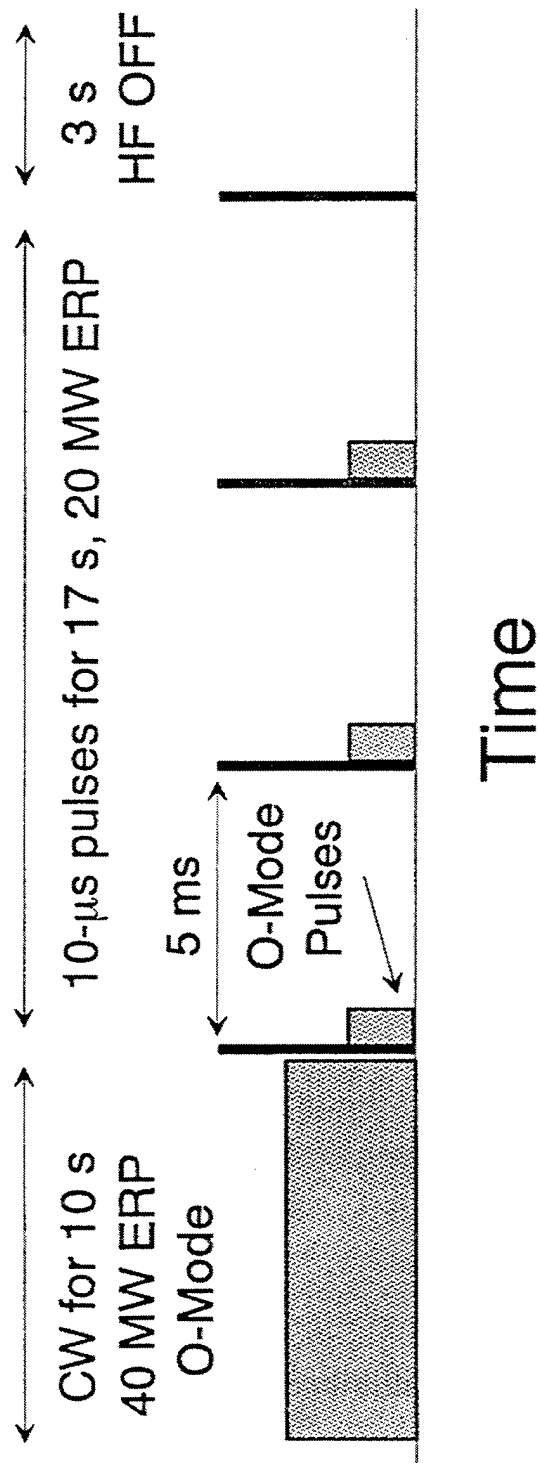


Figure 1. Pulse train used with the HIPAS HF facility for API studies. A continuous wave (CW) transmission lasting 10 s is used to modify the ionosphere. This was followed by a series of pulses 10- μ s in duration used to diagnose the atmosphere/ionosphere.

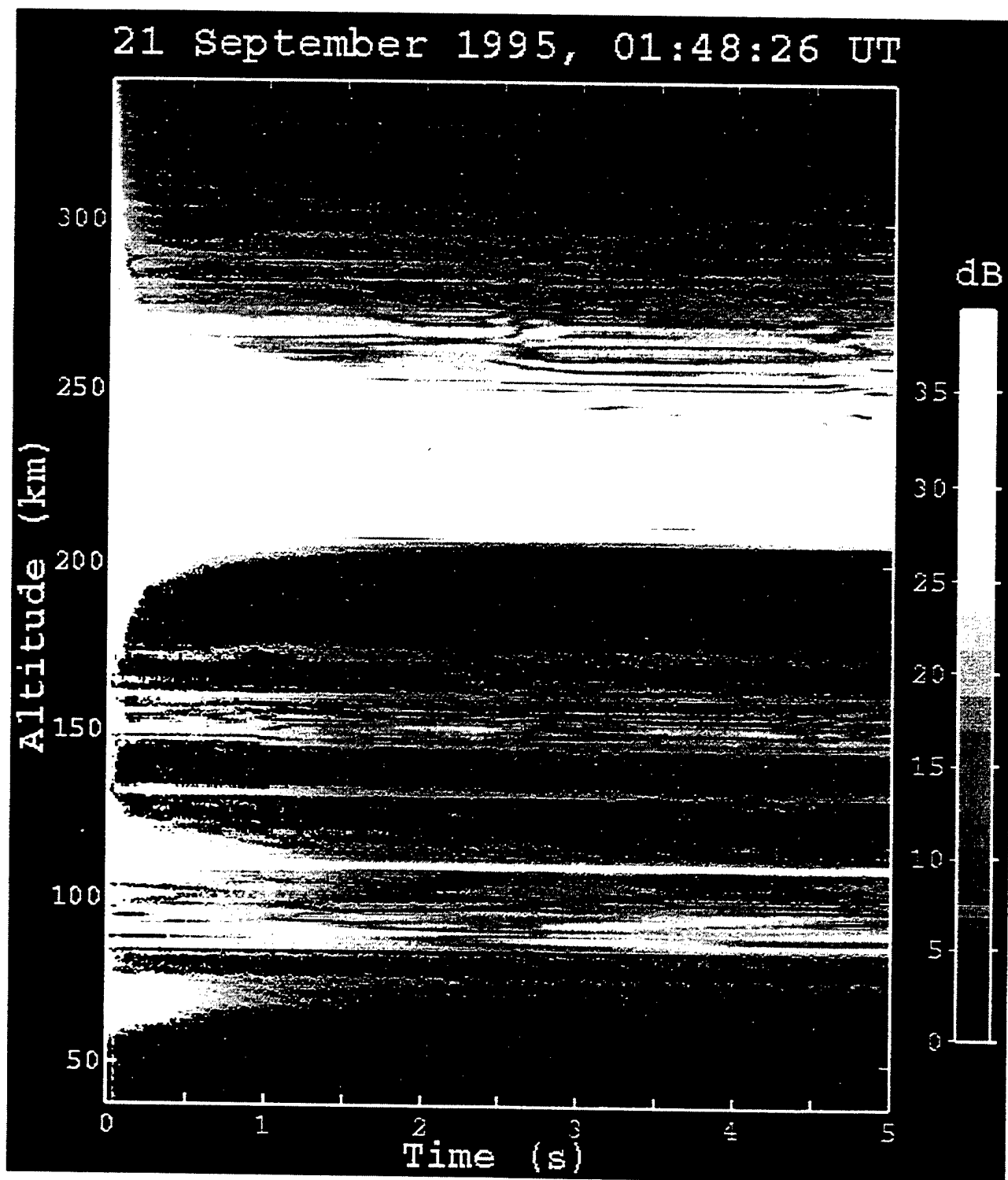


Figure 2. Range-time-intensity (RTI) plot illustrating the decay of API backscatter after modification transmissions are turned off. Time on the abscissa is referenced to HF turn-off and to the absolute time listed at top.

with time because the specular echo undergoes deep fading. Initially, very strong echoes are observed over wide range intervals extending from the range of specular return (206 km) down to ~170 km and to larger ranges above 340 km. These echoes are caused by API generated by ponderomotive forces near the point of reflection of the modifying HF wave. Similar results were first obtained at the Zimenki HF facility in Russia by *Belikovitch et al.* [1975] and much later at Arecibo Observatory, Puerto Rico by *Fejer et al.* [1984]. Echoes at virtual heights above the range of specular return are caused by the upward scattering of a small portion of the reflected diagnostic pulse by the API; the scattered wave subsequently reflects in the ionosphere and is received at a much longer range delay. The large range interval occupied by the F-region API scatter is in part caused by lower radio wave group velocities near the point of reflection. The actual height interval of strong API excitation below the point of HF reflection is much smaller than the virtual height interval of ~35 km shown in Figure 2. As in the case of the specular return, the F-region API saturates the HF receiver. The intensity decay constant of the *F* region API is ~60 ms, and after ~300 ms these echoes disappear. In the HIPAS experiments, decay constants are generally larger than those reported by *Belikovitch et al.* [1975] because of the lower frequency employed for modification.

Ionosonde measurements made with a Lowell Digisonde 256 were used to support the HIPAS observations. The Digisonde is located at a NOAA site near Gilmore, Alaska, approximately 34 km away from HIPAS Observatory. An ionogram obtained one minute after the observations of Figure 2 yielded an f_oF_2 value of 4.7 MHz; the real height of the *F* layer peak deduced from the ionogram was 261 km. Many echoes detected below the specular reflection height are of natural origin. Natural echoes tend to persist during the entire 5-s display of Figure 2 and typically exhibit Rayleigh fading statistics. The strong natural layer near 110 km altitude coincides with the bottom of the auroral E region as determined with the ionosonde, whereas the layer at 90 km is either a region of strong partial reflection or a patch of sporadic *E*. HF-induced signals have exponential decay curves; they are usually lost in the background noise within 1-2 s of HF turn-off at D-region/E-region altitudes and within ~0.5 s in the F region. Most natural echoes are the result of partial reflections from the ionosphere above HIPAS. Additionally, meteor echoes are occasionally detected along oblique ray paths. It is interesting to note that the echo at a range of 130.8 km in Figure 2 (red layer) probably corresponds to oblique scatter from a meteor. This echo is not observed in the HF pulsing sequences bracketing the observations of Figure 2 by ± 30 s. The measured Doppler shift of the echo is high (~40 m/s), consistent with it being of meteor origin. Most likely, the meteor is detected through the first sidelobe of the HF beam [*Wong et al.*, 1990], which yields a true height in the range 80 km - 100 km altitude.

In Figure 2 there is a small patch of HF-induced echoes near 150 km, but these signals quickly disappear. Longer lived echoes lasting a second or longer are observed at altitudes

between 60 and 130 km. Ionosonde measurements indicated that f_oE was ~ 2.45 MHz and the E region peak was located near 115 km altitude. API observed between 110 and ~ 125 km altitude are probably excited in the E layer. HF-induced echoes are often superimposed on scatter from natural partial reflection layers, patches of sporadic E , and scatter from the bottomside E layer. In the present work, particular attention is paid to API excited in the lower D region below ~ 80 km altitude. A discrete interval of lower D region backscatter is evident in Figure 2 between ~ 57 and ~ 76 km altitude. The altitude interval is largest immediately after the modifying HF pulse is turned off. With increasing time, the interval narrows and the echo retreats to the higher altitudes. The sharp upper edge of the scattering interval and the well-defined lower boundary is a characteristic feature of the HIPAS results. Weak backscatter from natural partial reflection layers is evident near the upper boundary. These echoes persist beyond the 5-s data interval displayed in Figure 2.

At a given height, one can determine the API intensity decay constant, τ_i , the initial power at HF turn-off, I_0 , and the phase history of the echo. Figures 3a, 3b, and 3c show time histories of echo power and phase at three mesospheric altitudes (62.4 km, 67.8 km, and 73.2 km). These results were obtained during the measurement period of Figure 2. The data were processed by coherently integrating signals from three consecutive range cells, which yields an effective range resolution of 1.8 km. At each range the API power decay curve and the signal phase history are fit using a nonlinear least-squares technique. The initial rapid decay of API power during the first 0.1 s of data is an artifact of the HF transmitter and is not analyzed in the HIPAS experiments. A surge in transmitter pulse output occurs when the system is switched from CW to pulsed operations. In Figure 3, calculations of I_0 and τ_i exclude the transmitter surge, and v_z denotes the phase velocity obtained from a linear fit. Solid lines refer to fitted data segments; dashed lines are simply linear extensions of these fits. At D region heights, the vast majority of the HIPAS echoes can be accurately fit to exponential decay curves and linear phase histories. A minor exception is shown in Figure 3c, where the dashed extension of the fitted phase curve begins to deviate from a linear trend after ~ 1.3 s. In this case, the underlying natural partial reflection echo appears to have a slightly different Doppler shift than the API echo. This difference becomes evident as the API echo decays away and the partial reflection echo becomes dominant.

Figures 3d and 3e illustrate time histories of echoes observed in the E region. The echo at 109.2 km is the result of API superimposed upon strong natural scatter. Observations shown at 118.2 km altitude correspond to API excitation in the E region with no natural underlying scatter. API measured at E region altitudes exhibit an exponential decay, but the phase history is not linear. This is similar to the case of natural E region scatter. A data segment showing F region API scatter at 303.6 km altitude is presented in Figure 3f. At this altitude, the HF receiver was not saturated. As in the E region, F region phase histories are nonlinear. In general, API layers generated in the E and F regions are easily distorted by natural electric fields. These spatial

21 September 1995, 01:48:26 UT

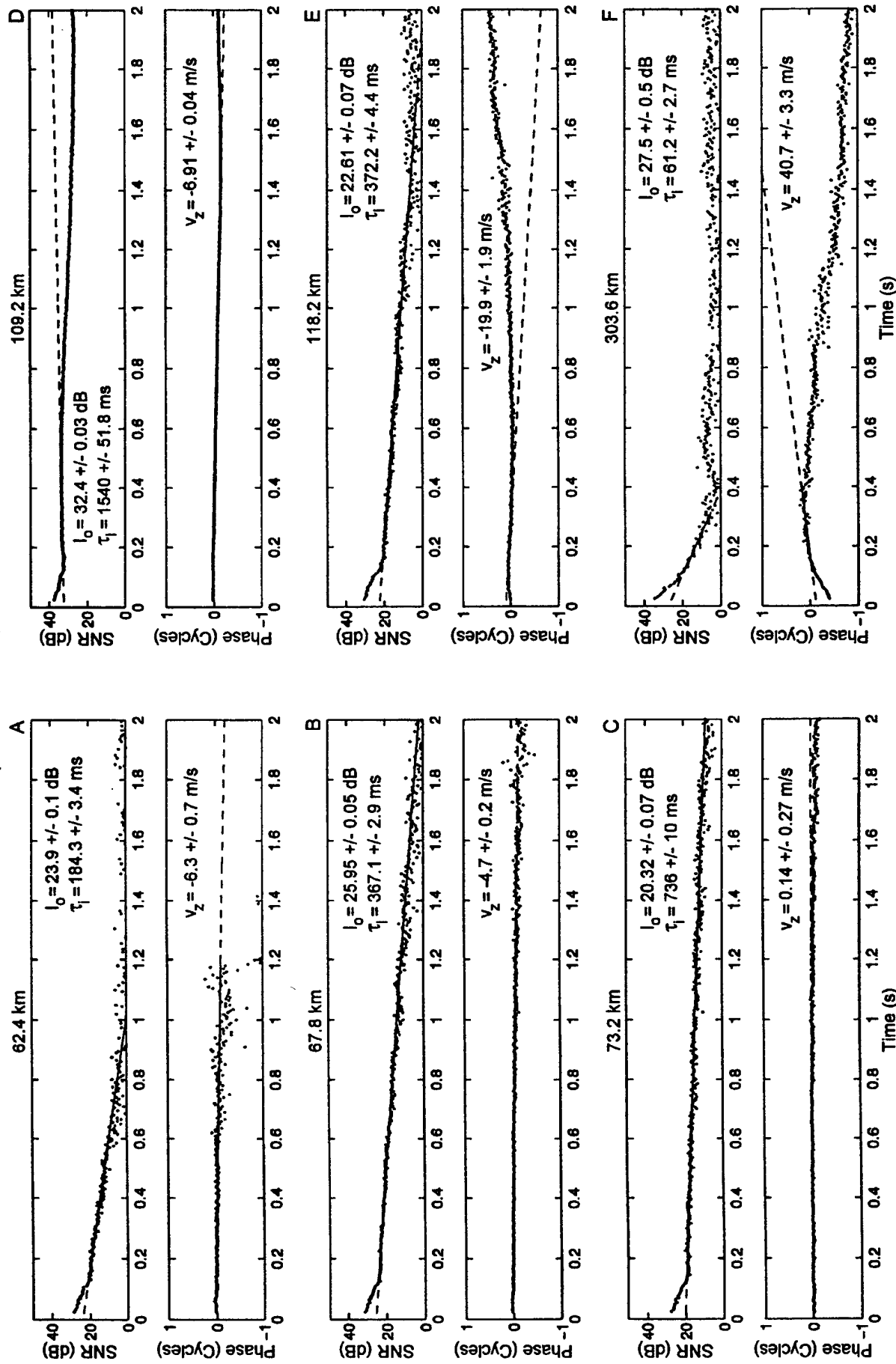


Figure 3. Power and phase histories of API backscatter obtained at six altitudes selected from the observations of Figure 2. Fitted values of echo power at HF turn-off (I_0) and the intensity decay constant (τ_i) are included in the power panels. In the phase panels, the fitted value of phase velocity is expressed in terms of vertical velocity (v_z). The errors bars listed are $1\text{-}\sigma$ values.

inhomogeneities can produce twisted phase histories and amplitude fading similar in nature to that observed with natural irregularities.

At D-region altitudes, where the API echoes are well-behaved, fitted results across an extended altitude interval are used to create profiles of phase velocity, decay constant, and peak signal power. Data from the observation period of Figure 2 are displayed in this format in Figure 4. Strong API signals are present from ~62 km to 75 km altitude. Least-squares fits to phase histories in this region are plotted as inferred vertical velocity v_z in the panel on the left. API echoes below 62 km were not of sufficient duration and amplitude to yield v_z values with small statistical error bars. Above 78 km, three points are included from natural partial reflection/sporadic *E* echoes that appeared to have linear phase histories for an extended period of time. In general, the v_z profile shown in Figure 4 is not unlike that expected for an internal gravity wave. Unfortunately, because of a loose phase-lock loop in a frequency synthesizer used with the HF facility, velocity profiles similar to that of Figure 4 are available only when absolute phase calibrations were made. Because such calibrations were infrequent, time series analyses cannot be used to probe the current data set for spectral features characteristic of gravity waves. This shortcoming will be eliminated in future experiments at HIPAS. However, under any circumstance additional validation studies are needed before the v_z results can be interpreted as direct measurements of vertical neutral wind velocity. In this regard, comparisons with incoherent scatter radar and/or Doppler lidar results are highly desirable.

In the center panel of Figure 4 the API decay constant is shown versus altitude, and on the right peak API power is displayed along with the average power of the natural echoes. Dotted lines connect data segments containing echoes of natural and artificial origin. A discrete region of strong lower *D* region scatter was routinely observed during the HIPAS campaign. The altitude extent of this region is generally of the order of 15-20 km. In Figure 4, this region is centered near 67 km. Notice that the decay constant is longer in the upper portion of the echo and that the decay time decreases with decreasing altitude. This decay constant profile is not unlike that reported by *Belikovich et al.* [1981]. During the HIPAS campaign, the center altitude of the *D* region scatter was observed to vary by as much as 15 km, or more than two neutral scale heights. An example of *D* region scatter observed in the vicinity of the stratopause at ~45 km altitude is shown in Figure 5. Just prior to this observation, the measured value of f_oF_2 was 4.30 MHz, and the deduced height of the *F* layer peak was 240 km. As in the case of Figure 2, the upper portion of the echo has a time constant near 0.5 s, and the time constant rapidly decreases with decreasing altitude. Significant changes in the echo altitude do not appear to alter the underlying temporal signature.

Efforts were made at HIPAS to determine the relative backscatter cross section of the lower *D* region API versus HF power. Observations were made over a 25 min period beginning at

21 September 1995, 01:48:26 UT

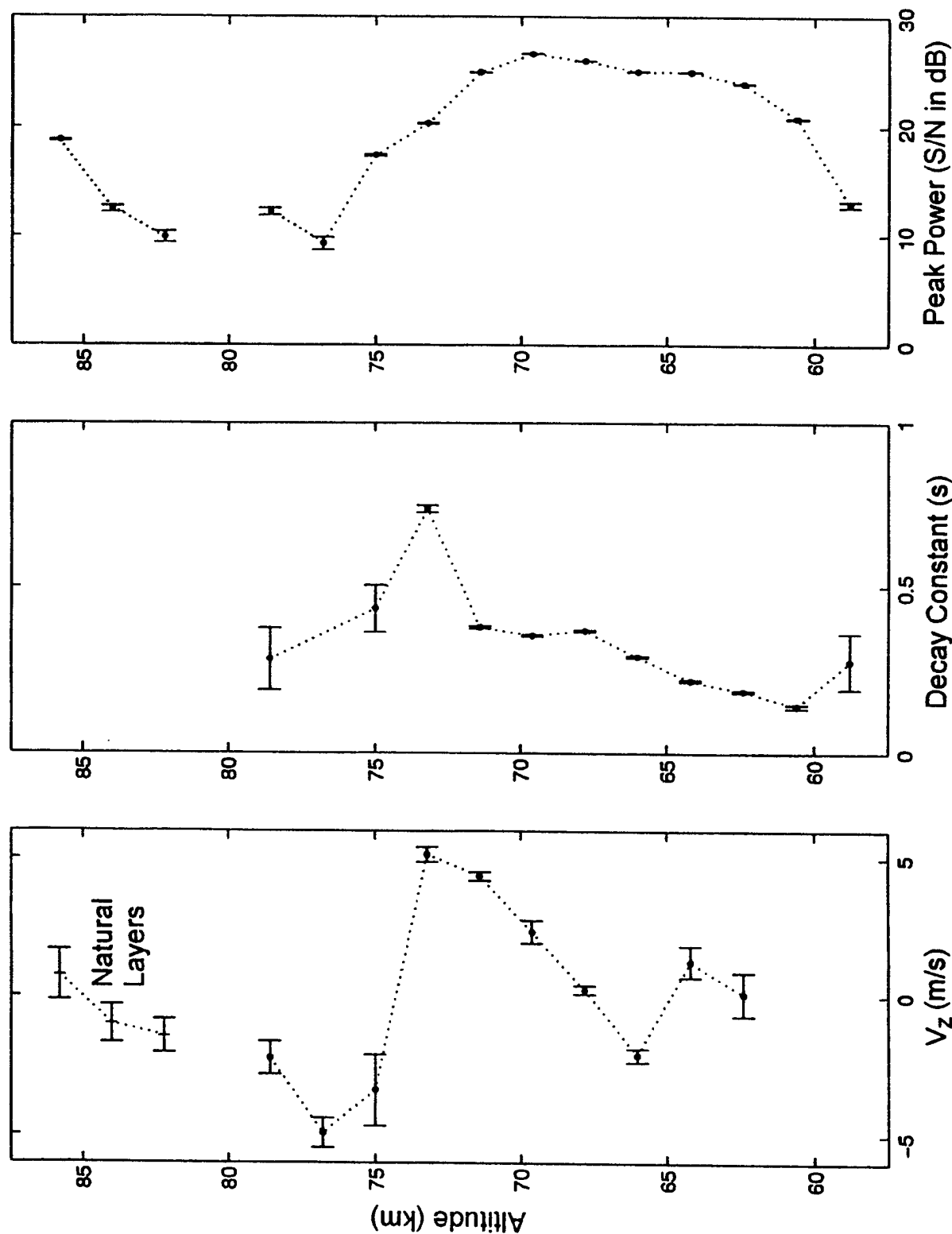


Figure 4. Altitude profiles of inferred vertical velocity v_z , intensity decay constant τ_i , and peak API power at HF turn-off I_o obtained for the observations of Figure 2. One-sigma error bars are plotted. Two altitude segments connected by dotted lines appear in the display. The lower segment consists of results from API echoes, whereas the upper segment makes use of natural partial reflection/sporadic E scatter to extend the altitude coverage of v_z .

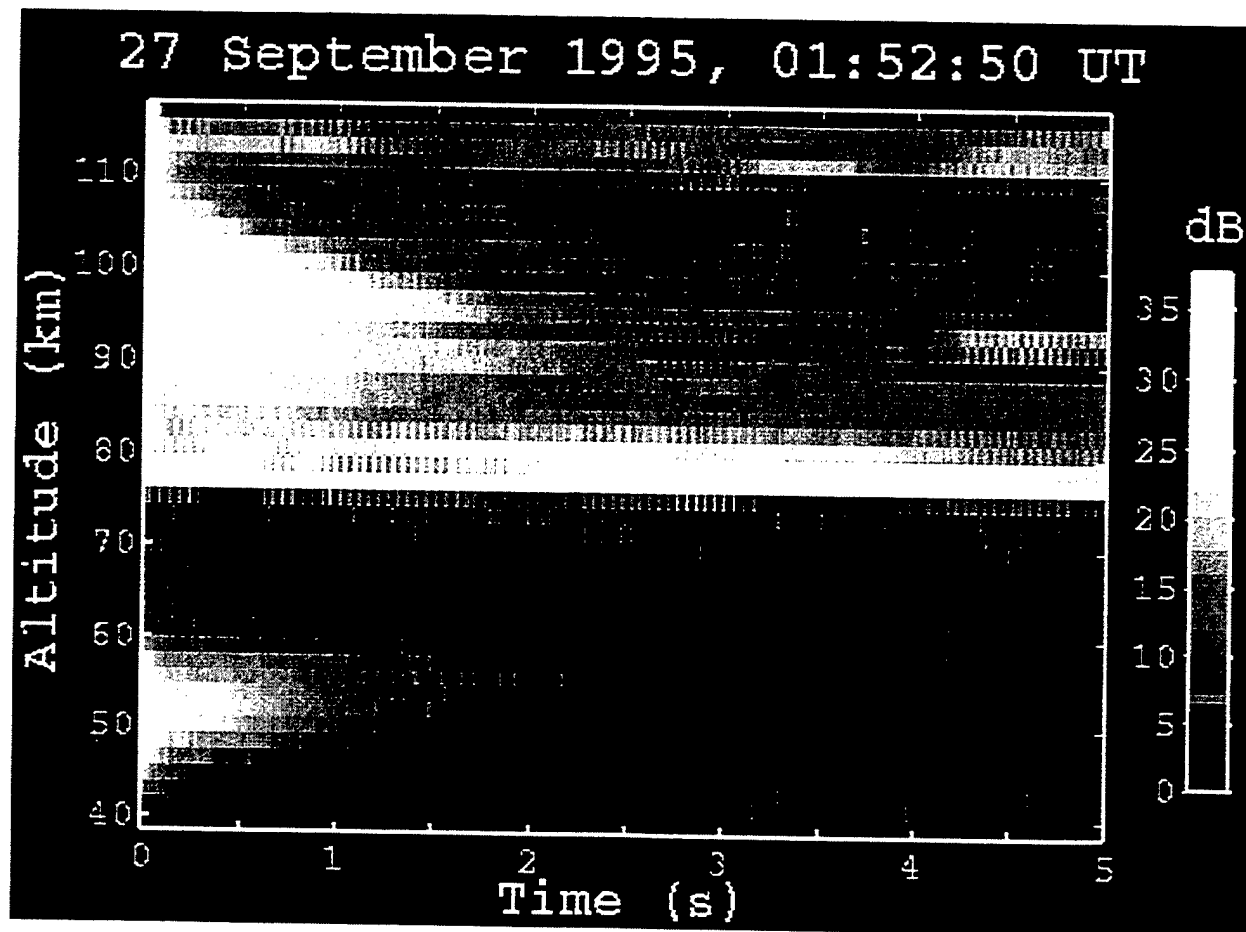


Figure 5. RTI plot of API excited deep in the atmosphere in the vicinity of the polar stratopause.

01:36:45 UT on 22 September 1995. During the measurement period, strong D region API scatter was observed between 63 and 72 km altitude. Figure 6 shows an RTI plot measured with 40 MW ERP at the beginning of the power stepping sequence. The ERP of the modifying HF wave, initially set to 40 MW, was stepped down to 20 MW, then to 10 MW, 4 MW, and finally to 2 MW, before being reset to 40 MW. Throughout the measurement period, the center altitude and the basic decay constant profile remained the same. Additionally, the F region ionosphere appeared to be relatively stable during the observations. Values of f_oF_2 obtained from the Digisonde ranged from 4.30 MHz to 4.40 MHz, and the deduced height of the F region peak varied between 255 and 265 km. The natural scatter observed between ~90 km and 120 km in Figure 6 appeared to dynamically change in the ionograms. However, at all times O-mode waves having frequencies ≥ 2 MHz penetrated the scattering region and reflected in the F region. It is unlikely that the 2.85-MHz modification wave suffered significant losses enroute to the F region.

Relative backscatter power versus ERP is presented in Figure 7. Measurements obtained in the 63-72 km altitude region were divided into three equal subintervals. The power stepping data were separately normalized to the 40 MW ERP result in each subinterval before they were combined to form the averages shown in Figure 7. Additionally, corrections have been made for the fact that diagnostic pulse power increases proportionally to modification pulse power. In the top panel, the average backscatter from all observations (open circles with dashed lines) is plotted together with the average backscatter from strong echoes above the 90 percentile level (filled circles with dotted lines). Other sorting and selection techniques were applied to the data (e.g., quartiles, 95 percentiles, median values, etc.), but the basic shape of the curve does not appear to depend greatly on the method of point selection or processing. Error bars shown reflect random errors of the nonlinear least squares fitting process. However, these error bars are much smaller than the random fluctuations of the data. The points that were used to calculate the overall average are shown in the bottom panel along with the average values shown at top as open circles. Note that the data in the bottom panel are displayed on a logarithmic scale. The variation in echo amplitude is quite large, and oftentimes signal strengths vary greatly from one modification pulse to the next. As indicated above, the temporal separation between pulses is 30 s. Most likely, the observed fluctuations in backscatter power are caused by fading of the HF reflected wave, which alters the standing wave ripple in the D region. This is discussed in greater detail below. Given the uncertainties introduced by the random fluctuations, one can conclude that the dependence of API backscatter on HF ERP is roughly linear in nature.

At HIPAS, API backscatter is often superimposed on natural scatter from partial reflection regions. This is in contrast with the experience at Tromsø [Rietveld *et al.*, 1996] where API echoes are not commonly observed together with partial reflection scatter. Figure 8 shows an example where the induced API echoes are mostly confined to partial reflection regions. No API

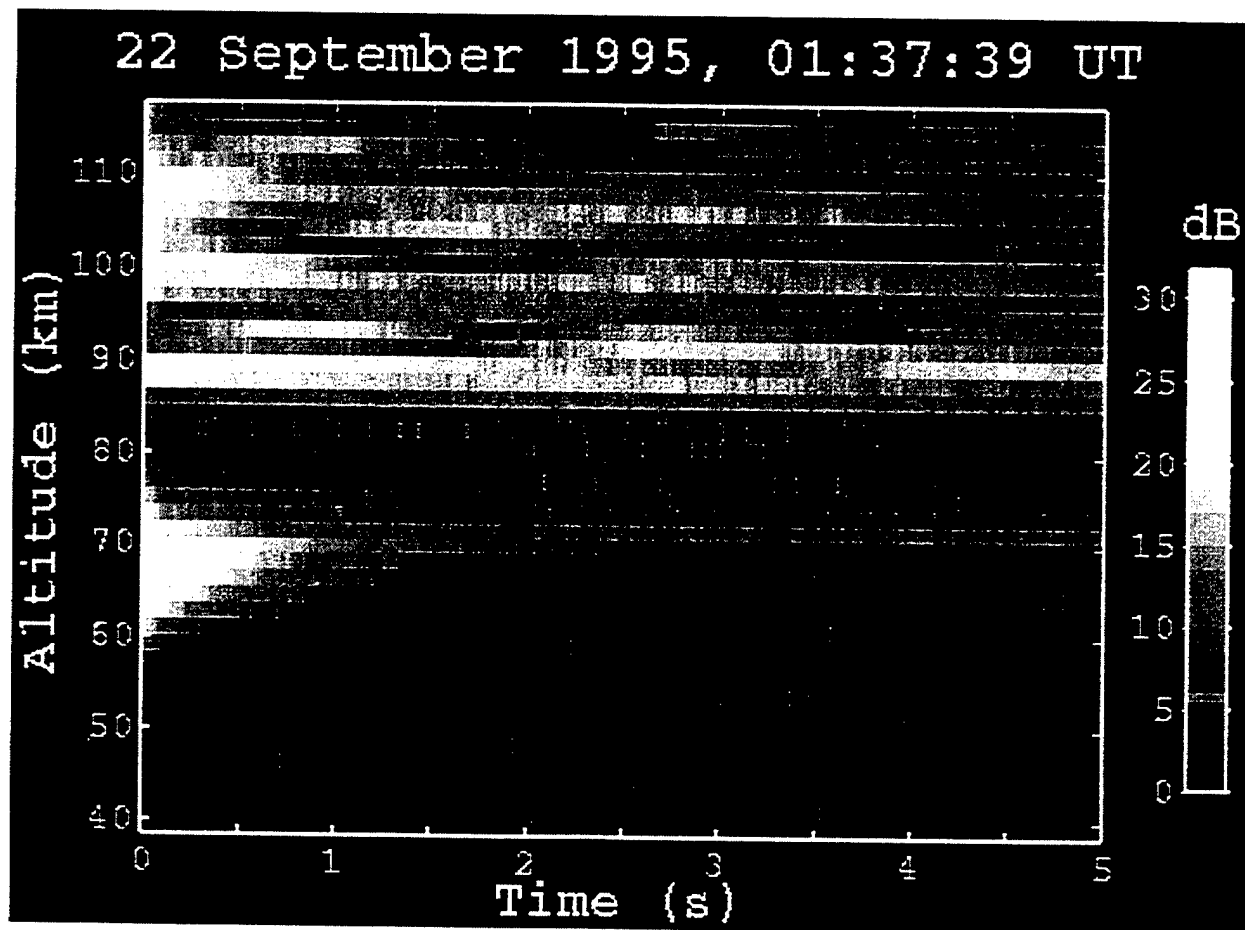


Figure 6. API measured at the beginning of a power stepping sequence with 40 MW ERP.

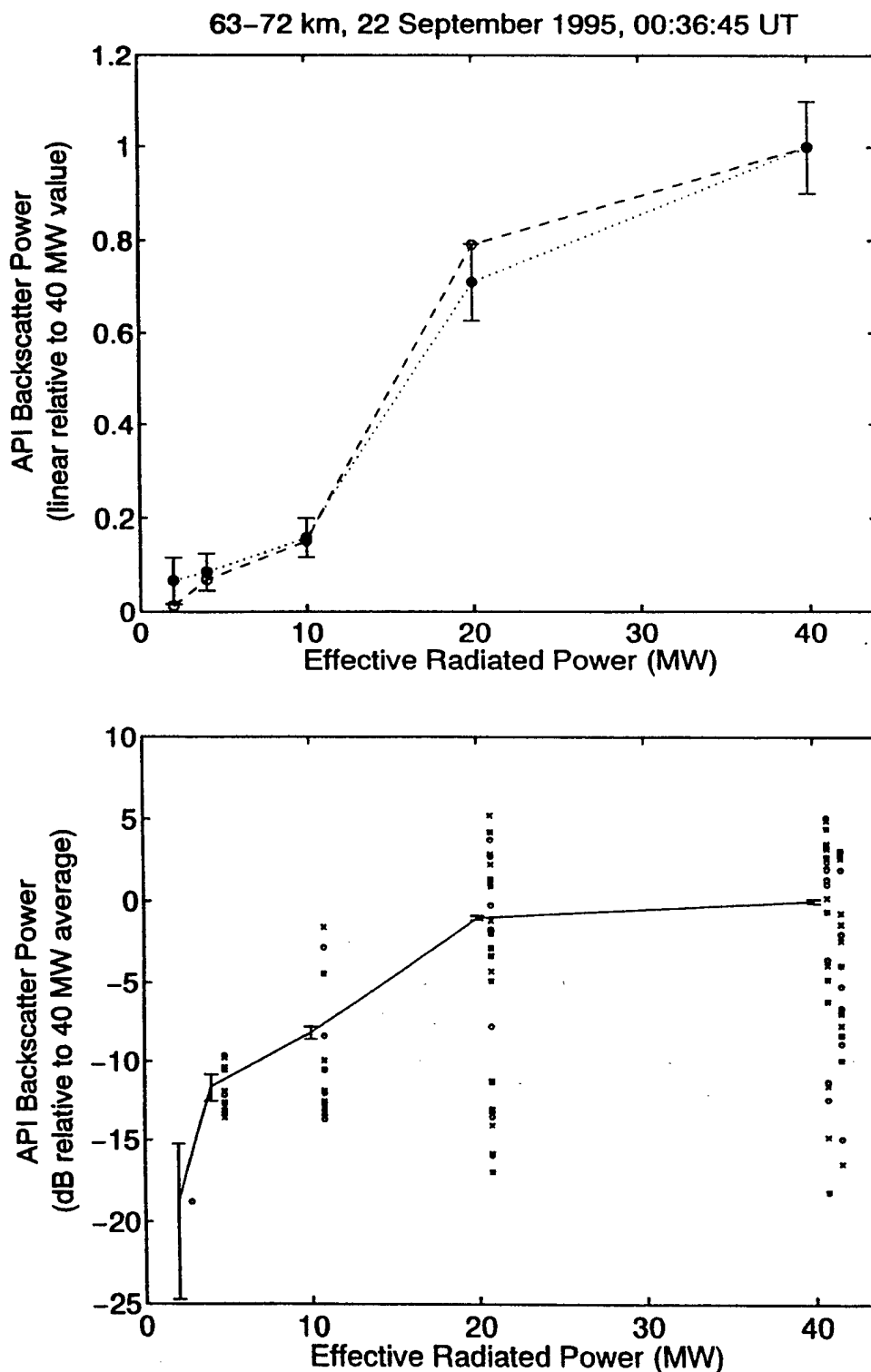


Figure 7. Dependence of API backscatter power on the power of the modifying HF transmissions. In the top panel, average API power is plotted as open circles, whereas the 90 percentile values are shown as filled circles. One-sigma error bars resulting from the measurement process are displayed. In the lower panel average API power is plotted on a logarithmic scale along with the data points used to determine the average. The symbols x, o, and * represent normalized data from altitude regions centered near 64, 67, and 70 km altitude. Strips of data points are displaced to the right of the average values for presentation purposes. Two separate data strips are shown at 40 MW ERP because two measurements were made, one at the beginning and one at the end of the power stepping sequence.

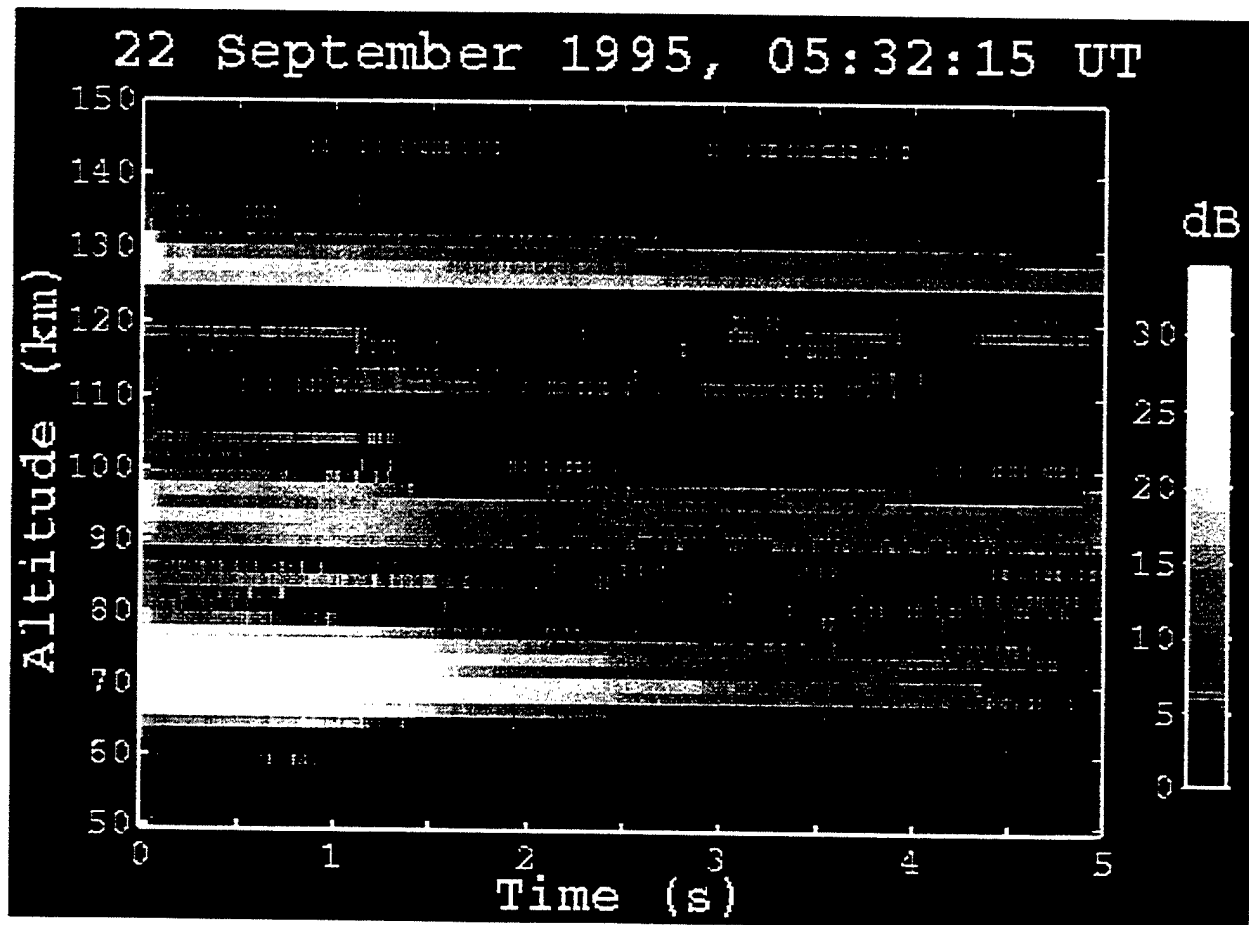


Figure 8. API scatter superimposed on natural partial reflection regions.

echoes were detected below 50 km. Prominent enhancements of natural echoes are seen in the 64-77 km altitude region. Weaker enhancements are apparent near 95 km and 127 km altitude. All three altitude regions contained persistent natural echoes, which exhibited the usual fading statistics of ionospherically scattered signals. An ionogram taken two minutes prior to these observations revealed a spread echo region between 95 km and ~150 km, consistent with the API results. O-mode waves having frequencies ≥ 1.5 MHz penetrated the scattering region and reflected in the F region. The measured f_oF_2 and the deduced height of the F region peak were 3.30 MHz and ~300 km, respectively.

2.4 Discussion

The initial HIPAS experiments confirmed several of the features of API echoes previously observed in the former Soviet Union, at Arecibo, Puerto Rico, and at Tromsø, Norway. During the campaign, particular attention was paid to API echoes in the lower mesosphere. Detailed observations made with 1.5-1.8 km altitude resolution indicate that the phase histories of the lower mesosphere echoes are strictly linear and the decay curves are strictly exponential. Vertical profiles of phase velocity yield results that are not inconsistent with the v_z component expected for vertical neutral motions in the mesosphere. However, detailed validation studies have not been performed at HIPAS, or any other facility, to verify that the phase velocities are a direct measurement of vertical neutral wind speed. Comparisons with Doppler lidar observations would be especially useful at altitudes between 50 and 70 km.

The HIPAS observations raised many additional questions that are not easily answered. The excitation of API in the D region is not uniform. Intense bands spanning 15-20 km in altitude are routinely observed. Typically, these bands exhibit a sharp upper edge and a well-defined lower boundary. The location of the band can vary by as much as 15 km, yet the temporal signature of the echo is not strongly dependent on the altitude of formation. Time constants for API decay are greatest near the upper boundary and decrease rapidly with decreasing altitude. This type of scattering profile is inconsistent with the smooth profiles obtained from modeling calculations in the past [e.g., *Belikovich and Razin*, 1986; *Rietveld et al.*, 1996]. It is clear that additional theoretical work is needed to explain this aspect of the HIPAS results.

Previously, a study of API time constants in the lower D region was performed by *Belikovich and Benediktov* [1986a]. These results were obtained with the Zimenki HF facility located near Nizhny Novgorad, Russia. Measurements were made with pulse widths of 50 μ s, which yielded an altitude resolution of 7.5 km, which is much coarser than at HIPAS. At a given height between 57 and 72 km significant fluctuations in decay constant are observed over timescales of tens of seconds. Moreover, altitude shifts of up to ~5 km are evident in plots of decay constant versus altitude on different observing days. The HIPAS results indicate that these shifts may be related to changes in the altitude of the scattering region. Displacements of the

scattering region in height would result in changes in the decay constant at a specific altitude. A seasonal variation is also reported by *Belikovitch and Benediktov* [1986a]. On average, the range interval over which the API time constant can be determined is shifted down in altitude by ~ 5 km in the winter. At altitudes between 60 and 70 km, values of the decay constant are smaller in the winter than in the summer; this difference becomes rather large (factor of three) near 70 km altitude. In general, changes in API decay constants are attributed to variations in neutral density and/or neutral temperature.

Belikovitch and Benediktov [1986b] show that the peak altitude of API echoes in the lower *D* region increases by ~ 15 km at sunset and that the lower boundary of the echo moves up in altitude by ~ 8 -9 km. Additionally, the echo time constants increase after sunset. This behavior is attributed to changes in the detachment rate of O_2^- . An interpretation of this nature is consistent with model calculations of the dependence of electron density and O_2^- profiles on solar zenith angle [e.g., *Ogawa and Shimazaki*, 1975]. However, an examination of the HIPAS data base indicates that the large day-to-day altitude shifts are not related to variations in solar zenith angle.

Particle precipitation could lead to significant changes in the altitude profiles of O_2^- and electron density, and thereby alter the altitude interval of the *D* region scatter. As noted earlier, the vast majority of all observations during the campaign were made under geomagnetic quiet conditions ($K_p \leq 2$) in the absence of substorms. In principle, precipitation associated with quiet time auroral arcs could play a role. Because the API observations were not made under dark sky conditions, no visual auroral data are available in this regard. However, magnetometer data from Alaskan stations at College, Poker Flat, and Fort Yukon were examined for evidence of particle precipitation. For a typical quiet time arc, one would expect to observe magnetometer fluctuations ≥ 40 nT over times scales of minutes. During most of the campaign, geomagnetic variations were of the order of 25 nT or less, except for a few instances when fluctuations were observed in the range 40-60 nT. For the observations presented in Figures 2, 5, 6 and 7, the average fluctuation levels at Poker Flat were 16 nT, 21 nT, 9 nT, and 10 nT, respectively. No correlation was found between the level of geomagnetic field variations and the height of the lower *D* region echo. This leads to the tentative conclusion that the altitude variations are not related to particle precipitation, at least not in a simple, straightforward manner.

At a constant HF power level, large (10-20 dB) fluctuations in the API echo strength are often observed over time scales of 30 s or less. This is probably caused by changes in the standing wave pattern in the *D* region. For the ionospheric conditions at HIPAS, the ripple on the *D* region pattern is no larger than 5% in power assuming low HF absorption and a smooth *F* region plasma. More realistically, natural and artificially-produced electron density fluctuations create an irregular reflection surface for the HF wave in the *F* region. As the associated perturbations in refractive index drift across the HF beam, and in particular across the first Fresnel zone (~ 6.5 km in diameter

at 200 km altitude) centered on the HF beam, a time varying diffraction pattern is generated at *D* region altitudes. Thus, one would expect resultant API echo strength to fluctuate from one modification pulse to another in a manner not unlike that of any ionospherically reflected radio wave. Moreover, the phase of the standing wave pattern will also change with time as the phase of the reflected wave varies. The amplitude and absolute phase of the API irregularities are most likely determined by the last few seconds of modification prior to the transmission of the diagnostic pulses.

Large variations in signal strength make it very difficult to perform controlled tests of API processes. Nevertheless, an attempt was made to determine the dependence of API amplitude on HF ERP. This yielded an approximately linear relationship up to the maximum power available for the tests (40 MW ERP). Under the assumption that an HF-induced electron-temperature "grating" is formed by the standing wave pattern of the modifying wave [e.g., *Belikovich and Benediktov*, 1986a], one has $\Delta N_e/N_e \propto \Delta T_e/T_e \propto \text{HF ERP}$, where N_e and T_e are electron density and electron temperature, respectively. Within this context, the linear power dependence simply indicates that electron thermal energy deposition in the lower *D* region is a linear function of HF power. This is not surprising because electron temperature nonlinearities caused, for example, by "thermal runaway" processes [*Perkins and Roble*, 1978] require HF power levels much greater than those available at HIPAS and preferably a modification frequency greater than that used in the current experiment. It should also be noted that the diagnostic pulse itself will cause a small amount of additional electron heating of the lower *D* region. However, this heating is uniform over spatial scales of the HF wavelength, and the pulse duration is too short to significantly change the background electron density profile.

API echoes are often detected at *E* region altitudes. However, in this region it is common for the HF-induced echoes to be superimposed on natural backscatter from partial reflection regions as well as scatter from auroral *E*/sporadic *E*. The interaction, if any, between processes responsible for natural scatter and API generation is currently not known. A partial reflection layer is occasionally seen near the top of the API region in the lower *D* region (Plates 1 and 3), but this does not appear to change the character of the API echo. Case studies such as the one presented in Figure 8 clearly illustrate that partial reflection regions and API can coexist.

API excited in the *E* region above HIPAS typically have intensity decay constants in the range of 60-100 ms, or amplitude decay constants of 120-200 ms. These results are consistent with the interpretation of *E* region relaxation times in terms of ambipolar diffusion. *Belikovich et al.* [1978b] report a 40 ms amplitude decay constant at a height of 120 km; this observation was made with a 5.65 MHz probe wave having O-mode polarization. The *E* region measurements of *Belikovich et al.* [1978b] are interpreted in terms of ambipolar diffusion. This yields an amplitude decay constant of

$$\tau_a = \frac{M_i v_{in}}{\kappa(T_e + T_i)k^2}, \quad (1)$$

where M_i is ion mass, v_{in} is ion-neutral collision frequency, κ is Boltzmann's constant, T_i is ion temperature, and k is vertical wavenumber.

Overall, the HIPAS *E* region decay constants are consistent with the ambipolar diffusion explanation. However, at first glance, the *E* region decay curves in Figure 2 between ~115 and 120 km appear to be too long to be explained by ambipolar diffusion. Figure 3e shows that at 118 km, the intensity decay constant is 372 ms yielding an amplitude decay constant of 744 ms. This is about four times greater than values of τ_a calculated from (1) using the free space value for k . The long time constant is probably caused by the lengthening of the radio wavelength near the peak of the *E* region. Ionograms obtained 34 km away from HIPAS indicated that f_oE was between 2.4 and 2.5 MHz. If this is representative of the *E* region at HIPAS, one has $f_{HF}/f_oE \sim 0.86$. For quasi-longitudinal propagation, one obtains $k/k_o \sim 0.5$, where k_o is the wavenumber in free space. Thus, the radio wavelength is roughly twice the free space value at the *E* region peak, and this increases τ_a by a factor of four. In Figure 2, the *E* region decay constant rapidly decreases with increasing altitude above ~118 km altitude. This is expected as the wave moves past the *E* region peak into regions of lower density plasma.

2.5 Conclusions

At altitudes between ~45 and ~80 km, high-resolution observations at HIPAS reveal the presence of well-defined bands of API scatter. Initially, the bands span an altitude interval of 15-20 km. However, shorter decay times prevail at lower altitudes giving rise to a characteristic retreat of the echo to higher heights. The echoes completely disappear over time scales of ~1-2 s. The discrete regions of *D* region scatter are difficult to explain within the context of existing theory. Additionally, variations in API altitude over ~15 km are not well-understood. Preliminary studies do not support a direct link between altitude fluctuations in the discrete *D* region patches and auroral particle precipitation. Further experimentation under dark and sunlit conditions is needed to verify the altitude fluctuations and investigate their origin. Power stepping studies in the *D* region reveal that a roughly linear relationship exists between API backscatter power and HF power. This is consistent with estimates of electron thermal energy deposition in the lower *D* region.

Large fluctuations in API backscatter power (10-20 dB) are typically observed in the *D* region over time scales of 30 s or less. Most likely, this arises because of fading in the ionospherically-reflected component of the standing wave pattern. Detailed modeling is required to quantitatively determine how temporal changes in the phase and amplitude of the standing wave impact API amplitude. Furthermore, the horizontal dimension of the API patch in the *D* region and the nature of its spatial structure are completely unknown. Ground-based HF interferometry

would provide much needed information in this regard. In the future, it is important that consistency checks be made between modeled API amplitudes and absolute API cross sections to verify source processes.

At HIPAS, API backscatter in the *D* and *E* regions is often superimposed on natural echoes from partial reflection regions, auroral *E* and sporadic *E*. The interaction, if any, between processes responsible for the natural scatter and API is currently not known. Echo decay rates in the *E* region provide a direct measurement of ambipolar diffusion. However, little, if any, information is contained in the *E* region phase history measured at a single receiver site.

Potentially, API can be employed as a powerful diagnostic tool for probing neutral motions throughout the mesosphere and across the turbopause boundary. However, detailed validation tests are needed to establish direct relationships between measured API parameters and atmospheric properties. Additional information about middle atmosphere chemistry is also likely to emerge as API observations and model results are compared in detail. For example, measurements at sunset and sunrise [Belikovich and Benediktov, 1986b] show an increase in the API decay constant in the lower mesosphere, which most likely is related to changes in O and excited [$\text{O}_2^1\Delta_g$]. The radiative lifetime of the latter is of considerable interest to theoretical studies of forbidden ground-state transitions in O_2 and is important for experimental investigations of upper-atmospheric ozone using O_2 infrared emissions [Pendleton et al., 1996; Mlynczak and Olander, 1995; Klotz et al., 1984].

2.6 Future Experiments

Experiments focusing on API production in the mesosphere will be performed at Arecibo Observatory, Puerto Rico following the completion of a new HF antenna system suspended above the reflector dish. Previously, no API observations have been made in the *D* or *E* region above Arecibo. Particular attention is being paid to the Arecibo experiments because of the quiescent environment that exists at this midlatitude location. It is hoped that controlled measurements can be made at Arecibo in the absence of large geomagnetic fluctuations. Moreover, natural partial reflection layers at Arecibo are expected to produce smaller echo returns than those encountered in the auroral region. This would reduce the clutter caused by natural irregularities and may make it easier to achieve a broader API altitude coverage. Arecibo Observatory offers a powerful incoherent scatter radar capable of monitoring vertical motions in the upper mesosphere (70-95 km altitude) with reasonably short integration periods. However, such radar observations are restricted to daytime hours when the *D* region is sunlit. At night, the Arecibo lidar system can be used to probe the neutral atmosphere between ~45 and 65 km altitude. Detailed validation studies are needed to clarify the relationship between vertical neutral motions and the v_z values obtained with the API technique. A central issue is whether the phase velocities of internal gravity waves influence the Doppler shift of the API. Important questions arise concerning the horizontal extent

of the API scattering region, and how it is structured. It is hoped that controlled experiments at Arecibo will allow the physical processes responsible for API generation to be critically examined and that it will be possible to characterize the API backscatter in greater detail.

If API phase histories can be used to directly measure vertical neutral motions, such observations will provide an important addition to MF radar techniques used to deduce neutral velocities from natural partial reflections. In the past, the Arecibo HF facility has been operated as an MF radar transmitter with great success [e.g., *Brosnahan and Adams*, 1993]. API echoes appear to be better suited for measurements of vertical velocity, whereas several MF radar techniques can be used to deduce horizontal neutral motions with some restrictions [e.g., *Hines et al.*, 1993]. Indeed, the API observing strategy is such that natural partial reflection measurements made with an HF interferometer are a necessary subset of the overall API observing process. *D* region API echoes decay over time scales of seconds; thereafter only the natural partial reflection layers remain.

Finally, we note that *Fejer* [1983] suggests a powerful diagnostic approach that could be used to measure absolute electron density perturbations associated with *F* region API. Because API gives rise to a spatially periodic medium, there is a substantial reduction in the group delay of probe waves having frequencies slightly greater than the modifying wave. This result is qualitatively interpreted in terms of a narrow stop band that develops at radio wavelengths near twice the spatial period of the API. The use of this technique would allow API electron density perturbations to be more easily measured in the *F* region plasma. Group delays could be conveniently determined by measuring signal phase as a function of frequency. Weak diagnostic waves could also be used in a bistatic arrangement to continuously monitor the evolution of API in the ionosphere.

3. Rocket Plume Studies from Wallops Island Flight Facility, Virginia

The rocket plume study consisted of a series of radar measurements aimed at examining the cross section and spectral signature of launch vehicle plumes. Particular attention is paid to determining the properties of the radar backscatter versus radar wavelength. To this end, we employed four radar systems operating at 49.92 MHz, 138.8 MHz, 430.0 MHz and 2.84 GHz. The 49.92 MHz radar used in this project was built for the HF Active Auroral Research Program (HAARP) by Geospace Research, Inc. (GRI) under contract NAS8-39238. A 40 kW, 138.8 MHz radar was provided by GRI for these studies. Finally, access to the 430.0 MHz and 2.84 GHz radars at Wallops Island Flight Facility was provided by NASA. Radar processors developed by GRI sampled baseband signals from the NASA 430.0 MHz and 2.84 GHz radars. This greatly aided efforts aimed at determining plume dynamics. The principal objective was to simultaneously record the spectral signature of rocket plumes at multiple radar wavelengths. In addition, attempts

were made to measure the polarization dependence of the echoes at VHF (i.e., 49.92 MHz and 138.8 MHz).

3.1 Background

In the past, the spectral characteristics of radar backscatter from rocket plumes has been examined in two missile tests conducted as part of the Boost Measurements and Analysis Program. These measurements were made at S-band. More recently, VHF and UHF radar measurements of missile plumes were made from White Sands Missile Range, New Mexico. The VHF experiment was performed as part of a collaborative effort between Geospace Research, Inc. and the Air Force Research Laboratory/Ionospheric Effects Division. The VHF measurements revealed the expected wideband plume signature, but the absolute cross section of the plume was significantly below model predictions. A second observation was made by MIT/Lincoln Laboratories using a UHF radar. Their results indicate that the plume cross section is somewhat greater at UHF. Unfortunately, a detailed characterization of the plume spectrum was not achieved in this experiment.

Because of the absence of an extensive data base, it is difficult to fully characterize the plume physics. Currently, it is believed that the highest velocity gases are generated close to the missile. These gases are shielded from most radar diagnostics because of the surrounding overdense plasma. Beyond the plasma critical surface there exists a large turbulent region containing partially ionized plasma. Most radars that operate in the VHF to UHF range detect incoherent backscatter from this part of the plume.

Complex numerical codes designed to simulate the plume composition, temperature/velocity and plasma content generally consist of three elements. The first addresses the combustion, thermodynamics, and fluid dynamics of gases at the rocket motor and nozzle. In effect, these reactions generate the source plasma that initializes the latter two stages of the code. The second calculational element addresses issues related to the outer plume velocity field, mixing layer combustion and growth, and chemical reactions in the ionized, collisional plasma. Finally, the interaction of an electromagnetic wave with the plume is calculated taking into account incoherent scattering from the hot randomly moving electrons in the highly collisional plume. Coherent backscatter from turbulent structures moving with the missile is not fully taken into account in most models. The important end items produced by the codes are the absolute radar cross section of the plume and its corresponding Doppler spectrum.

A comprehensive test program requires that radar measurements be made at different frequencies and aspect angles relative to the plume. By varying the radar wavelength one effectively probes different regions of the plume. For example, at VHF the probing wave is totally reflected near the outer plasma boundary, and the test wave is subject to significant collisional

absorption (which scales as f^{-2} in dB, where f is radar frequency). At S-band nondeviative collisional absorption is much less, and the wave penetrates into the inner region of the plume. Because the plume has a roughly cylindrical shape, the backscatter signal strength is strongly dependent on the incidence angle of the wave relative to the axis of the cylinder. By making multiple measurements at different aspect angles one can determine the shape of the scattering zone within the plume more precisely. Additional information about the shape of the scattering region can be obtained by simultaneously measuring the backscatter return at two different polarizations. This strategy makes use of differences in backscatter cross section versus E-vector alignment relative to, for example, the axis of a cylinder. If the E-vectors of two linearly polarized signals are aligned parallel (E_{par}) and perpendicular (E_{perp}) to the axis of the cylinder, the cross section at the E_{par} channel will generally be greater than the E_{perp} channel. The ratio of the two cross sections depends on the overall shape of the scattering region.

Finally, it is important to note that the plume chemistry changes as the missile moves to upper atmospheric heights. It is therefore of great interest to monitor the plume signature versus altitude through the engine cutoff event at high altitude. This provides a convenient means of monitoring the plume chemistry versus atmospheric pressure.

3.2 Radar Software and Hardware

In the past, analysis of data acquired with the new Datel Analog-to-Digital (A/D) data acquisition system has been limited by the absence of a utility to directly import a data file into MATLAB 4.x. A Windows-based utility called GetRec.DLL was developed to remedy this situation. This involved the use of the so-called Windows Applications Programming Interface. GetRec.DLL contains many features common to Windows Applications including an on-line Help Menu.

In preparation for the February/March 1995 campaign at Wallops Island Flight Facility, GRI provided technical support for the design, purchase, and mounting of yagi antennas for the 49.92 MHz and 138.8 MHz radar systems. This included the design of the antenna feed system, the layout of the radar beam switching unit, and the mechanical design of the antenna mounting system. Much of the mounting hardware was either purchased or constructed by GRI.

The February/March 1995 experiments required that three additional data-acquisition systems be brought on-line to support the radar observations and that an additional HAARP radar processor be modified for 14-bit complex signal processing. This task was successfully completed. The project involved hardware modifications to four Datel 14-bit analog-to-digital (A/D) boards owned by the Government for use in the HAARP style of processors. In addition, the HAARP processor software had to undergo several modifications because manufactured processor components have changed significantly since the construction of the HAARP units.

Finally, three new processor interfaces along with specialized connector cables were constructed for the data-acquisition systems.

The two radar field campaigns from Wallops Island Flight Facility were supported by Geospace Research, Inc. These entailed launches of two Aries rockets on February 12, 1995 and March 28, 1995. Technical advice was also provided by Geospace Research, Inc. for a similar launch on March 4, 1995. During the March 28, 1995 campaign, each of the VHF radars had dual transmit/receive switches and dual receiver channels so that backscatter from vertically and horizontally polarized signals could be simultaneously investigated. Indeed, these measurements served to define the scope of the experiment.

3.3 Radar Parameters

The rocket launches supported by Geospace Research, Inc. during this study are listed in Table 1 below along with radar frequencies and antenna configurations. The S-band and UHF radars (Spandar radars) are used for rocket tracking and atmospheric measurements by the Wallops Island Flight Facility. They serve as rocket range support diagnostics. The two VHF radars were deployed by Geospace Research, Inc. and the Air Force Research Laboratory; they were located in a trailer within 100 m of the S-band and UHF systems. The VHF radars were originally designed for use with the HF Active Auroral Research Program (HAARP) facility in Gakona, AK.

Table 1. Radars operated during Aries rocket launches in the first quarter of 1995. The antenna polarization is indicated by V (vertical) and H (horizontal). During the launch of March 28, 1995 the VHF1 and VHF2 antennas were configured so that the operator could manually switch between horizontal and vertical polarization.

Radar Frequency	Feb. 12, 1995	March 4, 1995	March 28, 1995
S-band (2840 MHz)	V	V	V
UHF (430 MHz)	V	V	V
VHF1 (138.8 MHz)	H	not used	H and V
VHF2 (49.92 MHz)	H	H	H and V

The above four radars were operated synchronously, and the same pulse repetition frequency (PRF) was used for all radars. Table 2 shows the characteristic parameters of each diagnostic radar used for the observations.

Table 2. Characteristic radar parameters

Frequency (MHz)	PRF (Hz)	Pulse Width (μ s)	Beam Width (3 dB points)	Antenna Gain (dBi)	Polarization	Power (kW)
2840	1280	1	0.39°	53	V	1000
430	1280	1	2.9°	36	V	5-1000
138.8	1280	5	30° × 30°	19	V or H	40
49.92	1280	5	30° × 30°	17	V or H	50

When viewing rocket plumes near the launch pad (4 km from radars), suitable adjustments had to be made to prevent saturation of the UHF and S-band receivers. This was accomplished by stepwise changes in transmitter power and front end receiver attenuation.

3.4 Rocket Plume Observations

The three ARIES rocket launches were part of the Navy's Light Exo-Atmospheric Projectile (LEAP) program. They provided targets of opportunity for plume measurements. All three rockets had beacon downlinks that allowed the two Spandar radars to automatically track the rockets. The VHF radars had two beam positions: one looking near the horizon (effectively a 3° elevation angle) at the launch pad and one positioned at an elevation angle of 10°. The VHF beams were repositioned manually during the course of the rocket flight.

Pulse-to-pulse Fast Fourier Transforms (FFTs) were used to obtain the rocket plume spectra. Typically, 512 pulses were used to form a spectrum and 5 spectra were integrated to yield an effective time resolution of about 2 s. Figure 9 shows a radar spectrum obtained with the 138.8 MHz prior to the launch (centered at T - 1 s) and at 4 s into the launch. The pre-launch spectrum represents background conditions, which includes contributions from time varying clutter sources. At T + 4 s, one observes the specular return from the rocket (sharp peak with negative Doppler shift) as it heads out over the Atlantic Ocean. The broad spectrum with a peak near +40 Hz is caused by the plume. In general, the plume echo extends across the entire spectrum, and there is a small amount of frequency aliasing at the highest and lowest (i.e. negative) frequencies. The ± 640 Hz spectra shown in Figure 9 correspond to ± 691 m/s in Doppler velocity. At 49.92 MHz, the plume spectrum is confined to about ± 200 Hz which corresponds to ± 600 m/s. The Doppler velocity bandwidths of the spectra are similar at 49.92 MHz and 138.8 MHz. At high frequencies (430 MHz and 2840 MHz) the spectra tend to be flat and featureless across the ± 640 Hz bandwidth. This is not inconsistent with the Doppler spread being independent of frequency. For example, at 430 MHz, ± 640 Hz corresponds to ± 223 m/s in Doppler velocity. If the plume echo extends approximately ± 600 m/s in Doppler velocity, then the

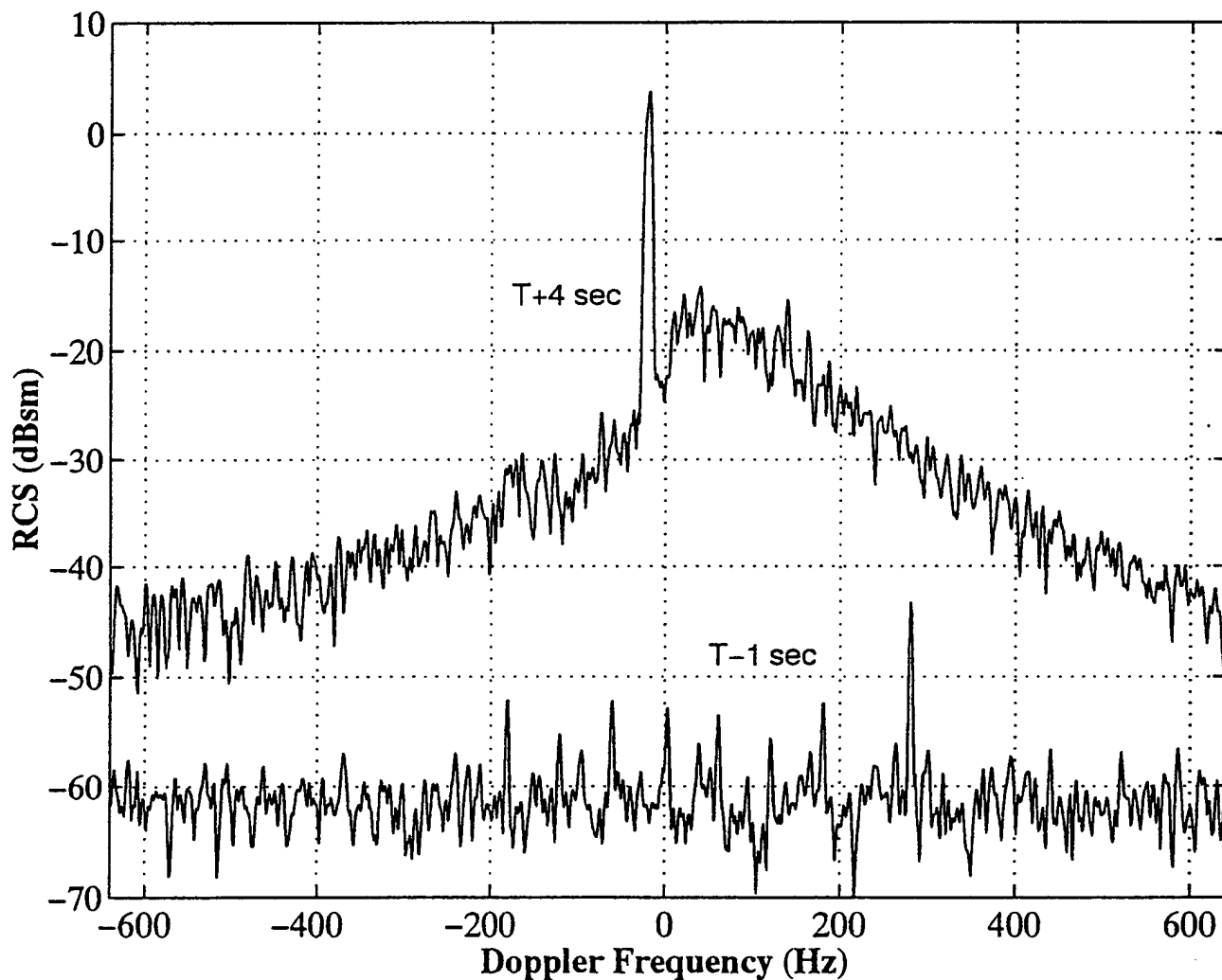


Figure 9. Spectral measurements of the Aries plume made at 138.8 MHz with horizontal polarization. The plot labeled T + 4 sec refers to observations made 4 seconds after launch, and T - 1 sec is the background spectrum recorded 1 second prior to launch. The sharp peak near the middle of the 4-second spectrum is the specular return from the body of the rocket. All other spectral components are caused by the plume.

plume echo will be aliased three times across the spectral bandwidth. This would serve to flatten the spectrum. Similar arguments can be made at 2840 MHz. In this case, the spectrum extends ± 33.8 m/s in Doppler velocity, and the alias factor is ~ 18 .

Absolute radar cross sections were obtained by calibrating the radars with jimspheres. Jimspheres are metalized balloons that are either tracked with the radars or allowed to drift upwards through the radar beam. For the February/March 1995 experiments, a 12" diameter jimsphere was used for cross section calibration of all four radar systems.

In this project, emphasis is placed on detection of low-altitude rocket plumes. A summary of the low-altitude cross section data is provided in Table 3 below. Plume signal was integrated across the spectral bandwidth to obtain the total cross section.

Table 3. Total plume cross section for an Aries Rocket

Frequency (MHz)	Feb. 12, 1995	March 4, 1995	March 28, 1995
2840	Receiver Saturated	Receiver Saturated	< -27 dBsm
430	Receiver Saturated	-16.8 dBsm	+5.6 dBsm
138.8, V polarization	Not Available	Not Available	-1.8 dBsm
138.8, H polarization	-3.1 dBsm	Not Available	-0.7 dBsm
49.92, V polarization	Not Available	Not Available	-15.0 dBsm
49.92, H polarization	-17.0 dBsm	-12.5 dBsm	-14.0 dBsm

March 28, 1995 was the only occasion when all radars and all available polarizations were measured. The observations indicate that there is very little difference in backscatter return for vertical and horizontal polarizations at 49.92 MHz and 138.8 MHz. Also the absolute cross section versus frequency tends to peak at UHF; at 49.92 MHz it is small, and at S-band it is very small. Except at 430 MHz, the total radar cross section appears to be consistent among different Aries launches (within 3 dB). It is not clear why there is a large difference in 430 MHz cross section between results obtained on March 4, 1995 and March 28, 1995.

In summary, it appears that the Doppler shifted spectrum of the Aries plume is confined to roughly ± 600 m/s relative to the radial Doppler velocity of the rocket. The same Doppler bandwidth is observed at 49.92 MHz and 138.8 MHz, and it is likely that a similar bandwidth exists at UHF and S-band. The total backscatter cross section does not appear to be sensitive to whether vertical or horizontal polarization waves are transmitted, at least at VHF. Finally, data obtained on March 28, 1995 suggests that the absolute plume cross section is greatest at UHF and declines at a moderate rate at higher and lower frequencies.

4. Equatorial Experiments from Chile

Support for radar operations during an observing campaign near the geomagnetic equator was provided by Geospace Research, Inc. between 23 September 1994 and 4 October 1994. This effort was part of a coordinated, multi-diagnostic investigation that was organized by the Ionospheric Effects Division of the Air Force Research Laboratory at Hanscom Air Force Base, MA. As part of the observing campaign, a 28-MHz radar was deployed at the main observing site near the town of Taltal, Chile. The radar beam was pointed perpendicular to geomagnetic field lines to measure aspect sensitive backscatter from field-aligned ionospheric irregularities. Within $\pm 20^\circ$ of the geomagnetic equator, a variety of natural physical processes gives rise to large-amplitude field-aligned irregularities in the ionospheric *F* region. The irregularities give rise to severe amplitude and phase scintillation in satellite downlinks at VHF, UHF, L-band, and beyond. The results of this and other similar equatorial campaigns are summarized by *Groves et al.* [1997]. Subsequent to the 1994 campaign, the HAARP 49.92 MHz VHF radar was modified so that the center line receiver and the plasma line receiver could be operated in a phase coherent manner. This was accomplished with the aid of an external frequency standard, which was power-divided and routed through the altered circuitry in each receiver. The system upgrade was motivated by the need to use interferometry techniques to better locate plumes of *F* region irregularities in the equatorial ionosphere.

5. Sprite/Blue Jet Campaign from Colorado

Radar support was provided to the Air Force Research Laboratory for an experimental investigation of lightning flashes in the upper atmosphere (stratosphere/mesosphere). The experiment field site was located at LaSalle Research Corporation, LaSalle, CO. The experiments were conducted during June and July 1997. The principal diagnostics were the HAARP 28 MHz radar and imaging CCD optics. Approximately 50 kW peak power was transmitted by the HAARP 28 MHz radar. The antenna was a steerable yagi array pointed at the horizon.

In the mid 1990s, a multi-disciplinary field emerged with the quantitative detection of spectacular "lightning" flashes above thunderstorms in the Midwest [e.g., *Sentman and Wescott*, 1993; *Lyons*, 1994]. To date, the principal diagnostics have been optical imagers, although similar events may also have been detected with VLF links [*Inan et al.*, 1995, 1996]. The objective of the study was to determine whether HF radio diagnostics are effective in measuring ionization created by "sprites" and "blue jets." These flashes extend from the tops of anvil clouds into the stratosphere and mesosphere. Because the physical processes involved are totally unknown, non-judgmental terms such as "sprites" and "blue jets" have been adopted to describe the phenomena. Sprites are blood red flashes that appear with bluish tendrils dangling from the bottom. These flashes last a few milliseconds and extend into the mesosphere (as high as 100 km altitude). The

blue jets are flashes that appear in narrow beams, sprays, fans, or cones of light which give off a blue or purple hue. They appear to originate at the top of the storm clouds and travel to altitudes of about 35 km; their speeds range from 30 to 100 km/s.

During the course of the Colorado campaign hundreds of sprites/blue jets were detected with the CCD imager. However, the principal result of the Colorado campaign was that no detections of sprites/blue jets were made with the HAARP 28 MHz radar. This indicates that very minor electron density perturbations are associated with sprites and blue jets.

The results of the Air Force Research Laboratory experiments are not unlike those obtained by Geospace Research, Inc. in a Midwest campaign conducted between June 1 through July 31, 1995. This campaign was funded by the National Science Foundation (NSF). The conclusion of the NSF study was that most sprites produce negligible forward scatter/reflection at HF. This is in stark contrast to the propagation of signals at VLF and LF. At VLF/LF, a causal disturbance collimated in the forward direction is consistently observed when sprites are generated within 50 km of the great circle propagation path.

The reason for the observed dependence on diagnostic frequency is evident from the model results of *Pasko et al.* [1996]. The predicted electron density in a sprite triggered by a positive stroke that discharges 200 C over a short period of time (~ 1 ms) is less than 10^3 cm^{-3} . This implies a stroke current of ~ 200 kA, which is near the high end of the distribution function of positive stroke currents. For reference, the largest sprite event during the NSF campaign involved a double sprite in which two sprites occurred within 50 km and were separated in time by three seconds. The peak currents of the first and second sprites were 148 kA and 137 kA, respectively.

It is possible that a significant portion of a 2.5 MHz signal could be forward scattered if a stroke with a very large (~ 400 kA) discharge current occurred along a propagation path or if a peak discharge rate near 300 kA occurred in conjunction with a long (tens of ms) continuing current. A sprite would have to produce a peak electron density of $2 \times 10^3 \text{ cm}^{-3}$ before it could be detected at the lowest HF frequency used in the experiment (2.5 MHz). On the other hand, VLF and LF signals are sensitive to much lower levels of ionization and are significantly perturbed by electron heating.

In conclusion, there is no evidence that sprites and blue jets produce detectable scatter in VHF or HF transmissions. The phenomenon produces interesting optical signatures but is typically accompanied by very small electron density perturbations ($< 2 \times 10^3 \text{ cm}^{-3}$).

6. HF Modification Experiment at Tromsø, Norway

An HF modification experiment was conducted at Tromsø, Norway in June 1998. The experiment made use of the high gain (30 dBi) HF array at Tromsø, which operates between 5.5 and 8.0 MHz. The half-power beamwidth is $\sim 7^\circ$. During the experiment, 1.2 MW of continuous

power was transmitted yielding an effective radiated power of 1.2 GW. The principal diagnostics were the European Incoherent Scatter (EISCAT) radars, which operate at 224 MHz and 933 MHz. These observations were complemented by measurements of stimulated electromagnetic emissions and ionospheric scintillation made by the Air Force Research Laboratory and Scion Associates. The campaign began on June 1, 1998 and was concluded on June 15, 1998. Approximately 100 hours of observing time were granted by EISCAT for this experiment. The participation of Geospace Research, Inc. in the campaign was funded jointly by the Air Force Research Laboratory and the NSF. The analysis of the radar data is supported by NSF.

6.1 Background

Over the past eight years, investigations of HF-induced Langmuir wave/ion wave turbulence have yielded many interesting results that reinforce the notion that our understanding of the wave-plasma interaction is far less than complete, particularly when HF-induced irregularities are present. Previous experimental investigations at Arecibo, Puerto Rico indicate that Langmuir waves detected with the 430 MHz incoherent scatter radar occur preferentially near the point of O-mode wave reflection. This observation together with Langmuir wave spectral data acquired at Arecibo led *DuBois et al.* [1990] to argue that radar measurements of initially excited Langmuir oscillations are consistent with computer simulations of strong Langmuir turbulence (SLT) near the region of critical density. Under conditions of SLT a significant fraction of the power in the high-frequency density oscillations is contained within highly localized states termed "cavitons." Cavitons consist of a high-frequency Langmuir field trapped in a self-consistent density depletion; they undergo cyclic nucleation, collapse, and burnout in the plasma. The theoretical study of *DuBois et al.* contained conclusions and predictions that sparked controversy and immediately triggered a new series of experimental tests.

A series of controlled experiments in the nighttime *F* region [*Djuth et al.*, 1990; *Fejer et al.*, 1991; *Cheung et al.*, 1992; *Sulzer and Fejer*, 1994] revealed that the initial HF beam-plasma interaction was consistent with the creation of strong states of plasma turbulence [e.g., *DuBois et al.*, 1990] in the *F* region. At the maximum power level available at Arecibo (~40 MW ERP prior to 1997), the predicted characteristics of strong turbulence in a smooth, inhomogeneous plasma appear to be present for 10-100 ms following HF turn-on (depending on HF power). Although there are some skeptics and critics of the strong turbulence interpretation, no other theory yields such a comprehensive and self-consistent description of the detailed data of *Fejer et al.* [1991] and *Sulzer and Fejer* [1994].

Many of the above findings involving strong states of Langmuir oscillations in ionospheric modification experiments are strongly disputed by *Stubbe et al.* [1992]. Using experimental results obtained with the Tromsø HF facility and the EISCAT UHF and VHF radars, *Stubbe et al.* show that propagating Langmuir and ion acoustic oscillations are an essential part of the physical

description at Tromsø and that parametric decay represents a major process in the production of Langmuir turbulence. They conclude that there is no convincing evidence at Tromsø that cavitons coexist with propagating Langmuir waves. However, more recently *Rietveld et al.* [2000] show results from Tromsø that are not unlike those recorded during the first 10 ms after HF turn-on at Arecibo. In addition, *Lee et al.* [1997] and *Kuo and Lee* [1999] dispute the existence of cavitons. They argue that most of the observed spectral structure can be interpreted as nonlinear scattering of parametric decay instability-excited Langmuir waves by "pre-existing" lower hybrid waves.

Despite the intense activity at Arecibo in monitoring Langmuir oscillations, much remains to be settled in this area of investigation. Most early-time (first 10 ms after HF turn-on) studies of Langmuir oscillations have been made at low HF powers (~40 MW ERP or less). Only a few observations were made at 80 MW ERP with the upgraded Isote facility before it was destroyed. During the first 10 ms of modification, the dependences of spectral features and instability growth times on altitude and transmitted HF power must be established with the new Arecibo heating system. In addition, more detailed measurements involving both the enhanced Langmuir oscillations and ion oscillations are necessary to resolve several existing theoretical controversies. For example, the space and time distribution of Langmuir turbulence described by *DuBois et al.* [1993a,b] predicts a zero frequency feature or a "filled in" center region of the ion line power spectrum that is directly related to caviton dynamics. In contrast, the theory of *Lee et al.* [1997] predicts the presence of two acoustic sidebands and no zero frequency feature.

The ultimate goal is to understand the excitation of Langmuir/ion oscillations over all time scales of modification. This is necessary in order to define the relationship between resonant instability development, the generation of Langmuir/ion oscillations, and the production of suprathermal electrons. However, the late time modification environment is quite complex. After ~50-100 ms of HF transmissions in a cold background ionosphere, the nature of the excited Langmuir oscillations appears to undergo a permanent change of state. It is thought that the change of state is related to the formation of HF-induced irregularities in the plasma. Over intermediate time scales of 50 ms to several seconds following HF turn-on, horizontally stratified irregularities and short-scale (3 - 6 m) field-aligned irregularities are generated in the plasma. The spectral characteristics of the Langmuir turbulence in this time domain have not been investigated in the past. However, such measurements are critical to the extension of Langmuir turbulence theory beyond the first 50 ms of modification. After 50 ms, the assumption of a smooth stratified plasma must be abandoned. Theoretical simulations become rather complex because heater-induced electron density perturbations must now be treated in a self-consistent manner. All possible theoretical formalisms cannot be explored in such a plasma environment. In this case, experimental investigations play an essential role in defining the direction of future theoretical inquiry.

6.2 Initial Results

As noted above, the most important observation involves measurements of the HF-enhanced ion line during the first 100 ms after the onset of the HF beam in the ionospheric F region. *DuBois et al.* [1993a,b] predict a zero frequency feature or a "filled in" center region of the ion line power spectrum while *Lee et al.* [1997] predict the presence of two acoustic sidebands and no zero frequency feature.

The advantage of testing the ion-line predictions at Tromsø is that the enhanced backscatter is about two orders of magnitude stronger than it is at a midlatitude station such as Arecibo. This is primarily due to the fact that the Tromsø observing geometry is nearly geomagnetically field aligned, and as a result large-amplitude, nonlinearly-driven, ion oscillations can be directly viewed. The disadvantage of performing such tests at Tromsø is that the auroral ionosphere is naturally more irregular than at midlatitudes. As a result, more patience is required at Tromsø if one is to observe wave plasma interactions in a smooth background plasma. One way to mitigate natural auroral irregularities is to perform experiments under sunlit conditions, that is, during the summertime. The high E region conductivity generated by the sun is not favorable for the maintenance of F region irregularities [e.g., *Vickrey and Kelley*, 1982; *Basu et al.*, 1987]. Indeed, this was one of the key motivations for performing the Tromsø experiments in June.

Figure 10 shows the development of the HF-enhanced ion line at Tromsø in a smooth, stable, F region plasma. A single 100 ms HF pulse was transmitted every 30 s. The very low duty cycle (0.33 %) was adopted to avoid pre-conditioning the plasma with HF-induced irregularities. Nevertheless, even at this low duty cycle, there were occasions when it did appear that pre-conditioning was occurring in the plasma. No pre-conditioning effects were detected during the observations of Figure 10. For these measurements, the HF modification frequency was set at 5.37 MHz and the HF effective radiated power was 1.2 GW.

The ion-line spectra of Figure 10 were obtained using the 224 MHz EISCAT radar. In this case, the radar beam was pointed vertically. A pseudo-random, phase-coded long pulse [e.g., *Sulzer*, 1986], was transmitted every 10 ms. The pulse was 1 ms in duration, and the baud length for 180° phase reversals was 1 μ s. It is generally accepted that the 224 MHz radar probes the plasma near the point of HF reflection (i.e. the critical layer) because of the small wavenumber of the diagnostic signal. The results of eleven 100-ms HF pulses were integrated to produce the spectra displayed in Figure 10. Altitude profiles of HF-enhanced ion line spectra are shown at times referenced to HF turn-on. Spectral power is plotted on a logarithmic scale. Noise baselines are determined by clutter generated by the spread spectrum radar coding technique. The first column of spectra versus range represents data acquired during the period 2 ms to 3 ms after HF turn-on. Successive spectral profiles are shown at 10 ms intervals set by the radar interpulse

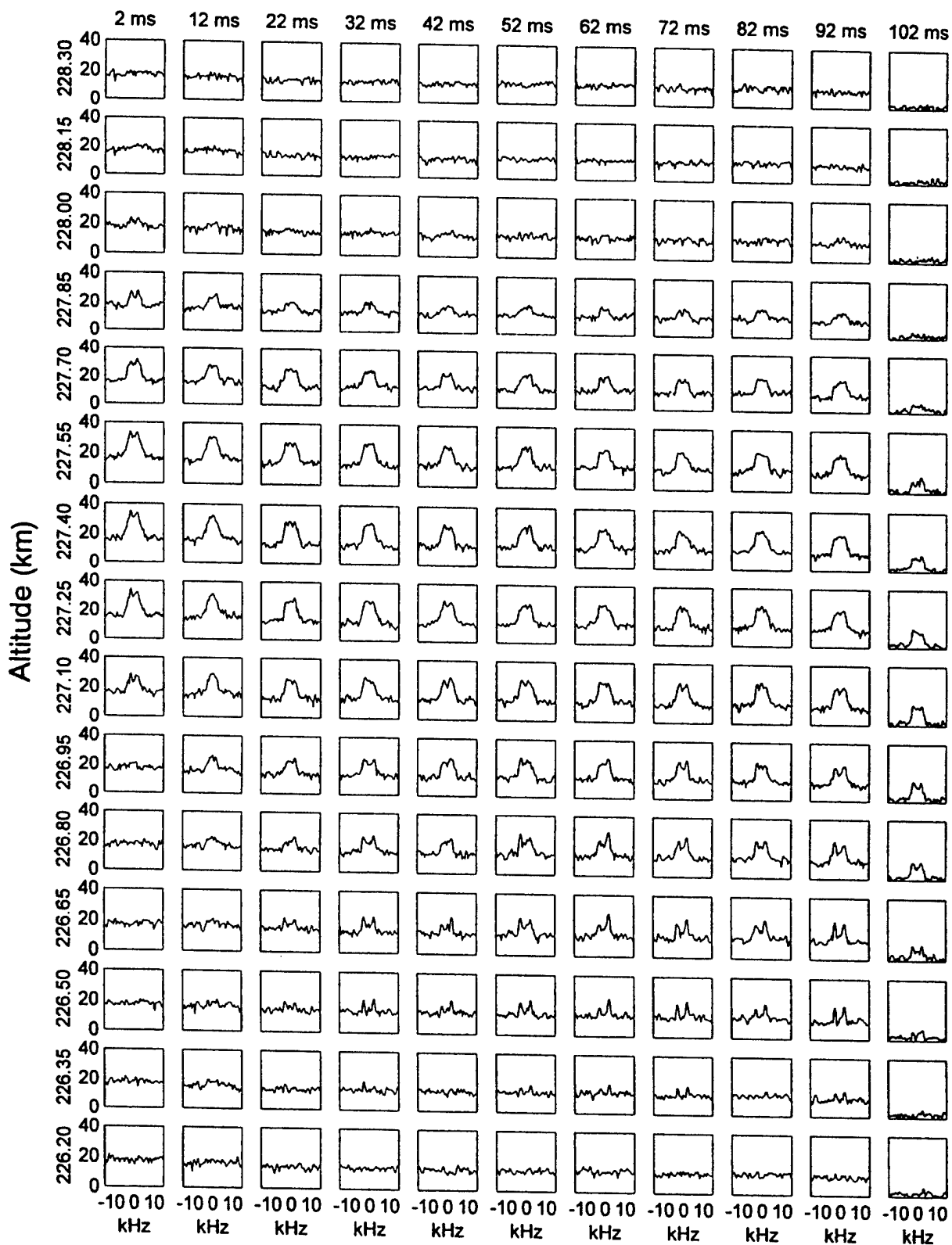


Figure 10. Temporal development of the HF-enhanced ion line monitored with the EISCAT 224 MHz radar. Spectral power is displayed on a logarithmic scale. Each column shows spectra versus altitude for a specific time relative to HF turn-on. The times are listed at the top of each column. HF turn-off in the plasma occurs at 100 ms relative time. These observations were made on June 13, 1998 between 06:33 and 06:38 UT.

period. The last column illustrates the decay of the ion line spectrum 2 ms after the HF beam is turned off. At the 150 m altitude resolution (i.e., 1 μ s baud) used for the measurements the natural incoherent scatter ion line is not detectable with the 224 MHz radar without prolonged data integrations.

Figure 10 shows that the strongest echoes are seen 2 ms after HF turn-on. This is the "overshoot" time constant in the plasma. Small acoustic sidebands are evident in most of the 2 ms spectra. Thereafter the spectra tend to be flat-topped, that is, the region between the acoustic sidebands is filled in. With increasing time the ion-line enhancements spread to lower altitudes. The spectra at the lowest heights are sharply double-peaked and there is a gradual transition between the double-peaked spectra at lower heights and the flat-top spectra at the greatest heights. Spectra obtained 2 ms after the HF beam is turned off (102 ms relative time) reveal a decay rate that is largest near the upper altitudes and smallest at the lower heights. The change in the baseline noise when the ion line decays is brought about by a reduction in clutter, which is proportional to echo strength. (See *Sulzer* [1986] for details.)

The results of Figure 10 are directly interpretable in terms of the theoretical work of *DuBois et al.* [1993a, b]. At 2 ms relative time, the broad spectrum with small acoustic peaks marks the initiation of the caviton production cycle. These spectra are observable from the critical altitude at 227.85 km down to 227.10 km. The caviton cycle involves cyclic nucleation of Langmuir oscillations in a density depression (the caviton) followed by the deepening of the cavity, collapse, and burn-out. The latter process is thought to give rise to electron acceleration in the plasma. The two small acoustic peaks are offset from the radar frequency by an amount that is about half the ion-acoustic frequency. This may indicate that the collapse events initially proceed subsonically. The "fill in" of the ion-line spectrum near zero frequency offset results from ponderomotively driven, off resonant, ion density fluctuations created during the nucleation and collapse process. At later times, the flat-top spectrum is dominant at altitudes between 227.25 km and 227.85 km. This is a clear signature of caviton collapse in the plasma. At low altitudes between 226.50 km and 226.80 km, one finds that the ion-line signal develops more slowly and that the spectrum is dominated by two ion-acoustic peaks. This is because resonant frequency-matching conditions are satisfied at these heights for excitation of the parametric decay instability. This instability process proceeds much slower than caviton collapse because of the weaker HF electric fields at lower altitudes and the coupling of Langmuir waves (i.e., driven waves) to heavily damped ion-acoustic waves. The parametric decay instability saturates by generating lower frequency, longer wavelength daughter waves known as a parametric cascade. In between the two altitude extremes is a gradual transition region between 226.80 km and 227.10 km altitude. In this region, free ion-acoustic waves produced by the parametric decay process coexist with "zero frequency" ion fluctuations caused by caviton collapse. When the altitude profile of the ion-

line spectrum is viewed at late times (e.g. 72 ms) one clearly sees the caviton collapse spectrum at the highest altitudes, followed by the transition or coexistence region where cavitons and parametric decay waves are both present, and finally the region where only parametric decay cascades occur at the very bottom.

As noted above, the HF-enhanced ion-line echoes tend to decay more quickly at higher altitudes when the HF electric field turns off in the plasma. This is because the cavitons rapidly decay in the absence of the HF electric field whereas the free ion-acoustic waves at lower altitudes decay at a rate determined by ion Landau damping. The latter rate is much smaller than the caviton decay rate. After the HF beam is switched off, no further cavitons can be nucleated and any cavitons caught in mid-cycle will quickly decay because of transit time damping.

In summary, the new Tromsø observations firmly support strong turbulence theory with caviton formation and indicate that the theories of *Lee et al.* [1997] and *Kuo and Lee* [1999] are less than complete. The work of *DuBois et al.* yields a self-consistent description of the early time development of ion and Langmuir oscillations in the plasma. Its final and complete experimental verification required the ion-line observations reported above. No other theory explains the experimental results obtained at Arecibo, Puerto Rico and Tromsø, Norway in such a comprehensive and self-consistent manner.

7. Radar Processor Upgrade

The existing HAARP radar processors were upgraded as part of this research program. In an effort to minimize both system hardware costs and software development costs, GRI selected a PC/PCI bus architecture with DOS 6.22 as the operating system. The upgrade entailed minor alterations to existing GRI hardware designs developed for the PC and significant changes in software previously written for the ISA bus. The overall idea was to use DOS to acquire and monitor data in real-time, and then use Windows 95 or Windows NT for data analysis on the same platform (if desired). A multiple boot program would allow DOS or Windows 95 to be selected at the time of boot up.

The new data acquisition system relies on the Dattel PCI-431C1B board. Each board has two pairs of data channels. Each channel on the Dattel card has a peak acquisition rate of 5 megasamples per second with 14-bit digitization. The Dattel board also contains a Texas Instruments floating point 320C44 50-MHz DSP microcomputer. This is a powerful DSP, but it has not yet been programmed for realtime processing. However, it must be programmed for any data acquisition activity including raw data taking. Accordingly, the current DSP software simply passes raw data through the DSP, and ultimately these data are stored as raw voltages on the hard drive. The Dattel card is configured with 0.512 MB x 32-bit SRAM. The SRAM can be upgraded

to a maximum of 2 MB x 32-bit. The added memory may be purchased independent of Datel. The SRAM is socketed on the PCI-431C board.

The data acquisition menu is identical to that of past HAARP processors. Most of the programming effort was directed toward rewriting large portions of the existing data-acquisition software for the PCI bus. As in the past, the source code is written in C and assembly language.

7.1 File Structure

Each data set is represented by two or three files. These files have the same eight character file name and each has one of three possible extensions: *.HDR, *.DAT, and *.ERR.

Header Files

This is a binary file that contains the parameters of the experiment: time, sample rate, number of samples, range gate, etc. It also contains information about which version of the data taking program was running, and some identifying information about the computer system on which it ran. This file is created before data taking commences. It is closed during data taking, and is reopened and updated at the end of the data run. It has the extension **.HDR** and is relatively small, only a few hundred bytes.

Data Files

This is a binary file that contains the actual acquired data; it has the extension **.DAT**. The data are divided up into records, one record per IPP. Each record has four header bytes. The first header byte will consist of bits read from a hardware register. The second header byte will be the echo count modulo 256. The third and fourth bytes are reserved for future use. The data samples for each channel follow the header bytes. They will be organized as follows: Channel 1I sample 1, channel 1Q sample 1, channel 2I sample 1, channel 2Q sample 1, channel 1I sample 2, channel 1Q sample 2 . . . channel 2Q sample N.

Error Files

Error files have the extension **.ERR**. They are optional text files. If there are no data acquisition errors, no error file is written. If an error occurs, the error file is written noting which IPP had the error and what the error type was.

7.2 Input Voltage Range

The full-scale input range for each analog channel is ± 2.5 V. All other features of the data acquisition system are the same as in the past.

REFERENCES

- Basu, Sa., E. MacKenzie, Su. Basu, E. Costa, P. F. Fougere, H. C. Carlson, and H. E. Whitney, 250 MHz/GHz scintillation parameters in the equatorial, polar, and auroral environments, *IEEE Comm.*, SAC-5, 102-115, 1987.
- Belikovich, V. V., and E. A. Benediktov, Measurements of the lower part of the *D* region of the ionosphere using artificial periodic inhomogeneities, *Radiophys.*, Engl. Trans., 29, 963-973, 1986a.
- Belikovich, V. V., and E. A. Benediktov, Artificial periodic nonuniformities in the lower part of the *D* region at sunset and sunrise, *Geomag. Aeron.*, Engl. Trans., 26, 705-706, 1986b.
- Belikovich, V. V., and E. A. Benediktov, The influence of temperature on the state of the plasma in the lower part of the *D* region of the ionosphere, *Geomag. Aeron.*, 26, Engl. Trans., 707-709, 1986c.
- Belikovich, V. V., and S. V. Razin, Formation of artificial periodic inhomogeneities in the *D* region of the ionosphere with attachment and recombination processes taken into consideration, *Radiophys. Quantum Electron.*, Engl. Trans., 29, 187-192, 1986.
- Belikovich, V. V., E. A. Benediktov, G. G. Getmantsev, Yu A. Ignat'ev, and G. P. Komrakov, Scattering of radio waves from the artificially perturbed *F* region, *JETP Lett.*, Engl. Transl., 22, 243-244, 1975.
- Belikovich, V. V., E. A. Benediktov, M. A. Itkina, N. A. Mityakov, G. I. Terina, A. V. Tolmacheva, and B. P. Shavin, Scattering of radio waves by periodic artificial ionospheric irregularities, *Radiophys. Quantum Electron.*, Engl. Transl., 20, 1250-1254, 1977.
- Belikovich, V. V., E. A. Benediktov, G. G. Getmantsev, M. A. Itkina, G. I. Terina, and A. V. Tolmacheva, Ionospheric electron density measurement using radio wave scattering from artificial plasma inhomogeneities, *Radiophys. Quantum Electron.*, Engl. Transl., 21, 853-854, 1978a.
- Belikovich, V. V., E. A. Benediktov, and G. I. Terina, Formation of quasiperiodic artificial inhomogeneities in the ionosphere, *Radiophys. Quantum Electron.*, Engl. Transl., 21, 985-988, 1978b.
- Belikovich, V. V., E. A. Benediktov, S. A. Dmitriev, and G. I. Terina, Artificial periodic plasma inhomogeneities in the lower part of the *D*-region ionosphere, *Izv. Vyssh. Uchebn. Zaved., Radiofiz.*, 24, 905-908, 1981.

- Belikovitch, V. V., E. A. Benediktov, Yu. K. Gol'tsova, G. M. Zhislin, G. P. Komrakov, and A. V. Tolmacheva, Determination of ionospheric parameters in the F region by the method of resonance scattering, *Radiophys. Quantum Electron.*, Engl. Transl., 29, 99-105, 1986.
- Belikovitch, V. V., E. A. Benediktov, and A. V. Tolmacheva, Measurements of electron density profiles in the ionosphere using artificial periodic inhomogeneities, in *The Upper Mesosphere and Lower Thermosphere: A Review of Experiment and Theory*, edited by R. M. Johnson and T. L. Killeen, pp. 251-254, AGU, Washington, DC, 1995.
- Borisov, N. D., and I. I. Varshavskiy, Effect of ionospheric inhomogeneities on radio-wave backscatter in an intense standing wave, *Geomag. Aeron.*, 22, 475-478, 1982.
- Brosnahan, J. W., and G. W. Adams, The MAPSTAR Imaging Doppler Interferometer (IDI) radar: description and first results, *J. Atmos. Terr. Phys.*, 55, 203-228, 1993.
- Cheung, P. Y., D. F. DuBois, T. Fukuchi, K. Kawan, H. A. Rose, D. Russell, T. Tanikawa, and A. Y. Wong, Investigation of Strong Langmuir Turbulence in Ionospheric Modification, *J. Geophys. Res.*, 97, 10575-10600, 1992.
- Djuth, F. T., R. J. Jost, S. T. Noble, W. E. Gordon, P. Stubbe, H. Kopka, E. Nielsen, R. Boström, H. Derblom, Å. Hedberg, and B. Thidé, Observations of E region irregularities generated at auroral latitudes by a high-power radio wave, *J. Geophys. Res.*, 90, 12293-12306, 1985.
- Djuth, F. T., M. P. Sulzer, J. H. Elder, High-resolution observations of HF-enhanced plasma waves in the Arecibo F region, *Geophys. Res. Lett.*, 17, 1893-1896, 1990.
- DuBois, D. F., H. A. Rose, and D. Russell, Excitation of strong Langmuir turbulence in plasmas near critical density: Application to HF heating of the ionosphere, *J. Geophys. Res.*, 95, 21221-21272, 1990.
- DuBois, D. F., A. Hanssen, H. A. Rose, and D. Russell, Space and time distribution of HF excited Langmuir turbulence in the ionosphere: comparison of theory and experiment, *J. Geophys. Res.*, 98, 17543-17567, 1993a.
- DuBois, D. F., A. Hansen, H. A. Rose, and D. Russell, Excitation of strong Langmuir turbulence in the ionosphere: comparison of theory and observations, *Phys. Fluids*, 5, 2616-2622, 1993b.
- Fejer, J. A., Method of remote sensing of horizontal stratification due to an ionospherically reflected powerful radio wave, *J. Geophys. Res.*, 88, 489-492, 1983.
- Fejer, J. A., F. T. Djuth, and C. A. Gonzales, Bragg backscatter from plasma inhomogeneities due to a powerful ionospherically reflected radio wave, *J. Geophys. Res.*, 89, 9145, 1984.

- Fejer, J. A., M. P. Sulzer, and F. T. Djuth, Height dependence of the observed spectrum of radar backscatter from HF-induced ionospheric Langmuir waves, *J. Geophys. Res.*, **96**, 15985-16008, 1991.
- Groves, K. M., S. Basu, E. J. Weber, M. Smitham, H. Kuenzler, C. E. Valladares, R. Sheehan, E. MacKenzie, J. A. Secan, P. Ning, W. J. McNeill, D. W. Moonan, and M. J. Kendra, Equatorial scintillation and systems support, *Radio Sci.*, **32**, 2047-2064, 1997.
- Hines, C. O., G. W. Adams, J. W. Brosnahan, F. T. Djuth, M. P. Sulzer, C. A. Tepley, and J. S. Van Baelen, Multi-instrument observations of mesospheric motions over Arecibo: comparisons and interpretations, *J. Atmos. Terr. Phys.*, **55**, 241-287, 1993.
- Inan, U. S., T. F. Bell, V. P. Pasko, D. D. Sentman, E. M. Wescott, and W. A. Wescott, VLF signatures of ionospheric disturbances associated with sprites, *Geophys. Res. Lett.*, **22**, 3461-3465, 1995.
- Inan, U. S., A. Slingeland, V. P. Pasko, and J. V. Rodriguez, VLF and LF signatures of mesospheric/lower ionospheric response to lightning discharges, *J. Geophys. Res.*, **101**, 5219-5237, 1996.
- Klotz, R., C. M. Marian, S. D. Peyerimhoff, B. A. Hess, and R. J. Buenker, Calculation of spin-forbidden radiative transitions using correlated wave functions: lifetimes of $b^1 \Sigma^+$, $a^1 \Delta$ states in O_2 , S_2 , and SO , *Chem. Phys.*, **89**, 223-236, 1984.
- Kuo, S. P., and M. C. Lee, On the generation of a broad downshifted spectrum of HF wave enhanced plasma lines in the ionospheric heating experiments, *Geophys. Res. Lett.*, **26**, 3289-3292, 1999.
- Lee, M. C., *et al.*, Laboratory reproduction of Arecibo experimental results: HF wave-enhanced Langmuir waves, *Geophys. Res. Lett.*, **24**, 115-118, 1997.
- Lyons, W. A., Characteristics of luminous structures in the stratosphere above thunderstorms as imaged by low-light video, *Geophys. Res. Lett.*, **21**, 875-878, 1994.
- Mlynarczyk, M. G., and D. S. Olander, On the utility of the molecular oxygen dayglow emissions as proxies for middle atmospheric ozone, *Geophys. Res. Lett.*, **22**, 1377-1380, 1995.
- Ogawa, T., and T. Shimazaki, Diurnal variations of odd nitrogen and ionic densities in the mesosphere and lower thermosphere: Simultaneous solution to photochemical-diffusive equations, *J. Geophys. Res.*, 3945-3960, 1975.
- Pasko, V. P., U. S. Inan, and T. F. Bell, Sprites as luminous columns of ionization produced by quasi-electrostatic thundercloud fields, *Geophys. Res. Lett.*, **23**, 649-652, 1996.

- Pendleton, W. R., D. J. Baker, R. J. Reese, and R. R. O'Neil, Decay of $O_2(a^1 \Delta_g)$ in the evening twilight airglow: Implications for the radiative lifetime, *Geophys. Res. Lett.*, **23**, 1013-1016, 1996.
- Perkins, F. W., and R. G. Roble, Ionospheric heating by radio waves: Predictions for Arecibo and the satellite power station, *J. Geophys. Res.*, **83**, 1611-1624, 1978.
- Rietveld, M.T., E. Turunen, H. Matveinen, N. P. Goncharov, and P. Pollari, Artificial periodic irregularities in the auroral ionosphere, *Annales Geophysicae*, **14**, 1437-1453, 1996.
- Rietveld, M. T., H. Kohl, B. Isham, C. La Hoz, and T. Hagfors, Measurements of HF enhanced plasma and ion lines at EISCAT with high altitude resolution, *J. Geophys. Res.*, in press, 2000.
- Sentman, D. D., and E. M. Wescott, Observations of upper atmospheric optical flashes recorded from an aircraft, *Geophys. Res. Lett.*, **20**, 2857-2860, 1993.
- Stubbe, P., H. Kohl, and M. T. Rietveld, Langmuir Turbulence and Ionospheric Modification, *J. Geophys. Res.*, **97**, 6285-6297, 1992.
- Sulzer, M. P., A radar technique for high range resolution incoherent scatter autocorrelation function measurements utilizing the full average power of klystron radars, *Radio Sci.*, **21**, 1033-1040, 1986.
- Sulzer, M. P., and J. A. Fejer, Radar spectral observations of HF-induced ionospheric Langmuir turbulence with improved range and time resolution, *J. Geophys. Res.*, **99**, 15035-15050, 1994.
- Vickrey, J. F., and M. C. Kelley, The effects of a conducting *E* layer on classical *F* region cross-field diffusion, *J. Geophys. Res.*, **87**, 4461-4466, 1982.
- Wong, A. Y., and R. G. Brandt, Ionospheric modification - An outdoor laboratory for plasma and atmospheric science, *Radio Sci.*, **25**, 1251-1267, 1990.
- Wong, A. Y., J. Carroll, R. Dickman, W. Harrison, W. Huhn, B. Lum, M. McCarrick, J. Santoru, C. Schock, G. Wong, and R. F. Wuerker, High-power radiating facility at the HIPAS Observatory, *Radio Sci.*, **25**, 1269-1282, 1990.